

RESEARCH ARTICLE

10.1002/2016JA022435

Key Points:

- Production and densities in Martian ionosphere
- Six new flare responses in the Martian ionosphere
- Modeling of X-ray aeronomy of Mars

Correspondence to:

S. A. Haider,
haider@prl.res.in

Citation:

Haider, S. A., I. S. Batista, M. A. Abdu, A. M. Santos, S. Y. Shah, and P. Thirupathaiah (2016), Flare X-ray photochemistry of the *E* region ionosphere of Mars, *J. Geophys. Res. Space Physics*, 121, 6870–6888, doi:10.1002/2016JA022435.

Received 1 FEB 2016

Accepted 18 JUN 2016

Accepted article online 22 JUN 2016

Published online 15 JUL 2016

Flare X-ray photochemistry of the *E* region ionosphere of Mars

S. A. Haider^{1,2}, I. S. Batista¹, M. A. Abdu^{1,3}, A. M. Santos¹, Siddhi Y. Shah², and P. Thirupathaiah²

¹Aeronomy Division, Instituto Nacional de Pesquisas Espaciais, São José dos Campos, Brazil, ²Space and Atmospheric Sciences, Physical Research Laboratory, Ahmedabad, India, ³Division of Electronic, Instituto Tecnológico de Aeronautica, São José dos Campos, Brazil

Abstract Based on electron density profiles obtained from the Mars Global Surveyor (MGS) we report X-ray flare responses in the *E* region ionosphere of Mars during six events that occurred on 28 March and 6 April 2001, 17 and 18 March and 21 April 2003, and 19 February 2005. We have developed a time-dependent Analytical Yield Spectrum model to calculate a time series of photoionization rate, photoelectron impact ionization rate, photoelectron flux, ion density, electron density, and ionospheric electron content (IEC) of the *E* region for each flare day. The estimated production rate, flux, and densities increase by 1–2 orders of magnitude due to effect of these flares in the *E* region ionosphere of Mars. The estimated IEC are compared with the measured IEC. It is found that the normalized IEC of the simulated *E* layer increased by a factor of 5–10 at the flare time compared to a factor of 2 enhancements in the normalized IEC of the corresponding MGS profiles.

1. Introduction

During 1965 to 1980, 443 electron density profiles were observed by radio occultation experiment from various Mars' missions [Mendillo *et al.*, 2006]. Radio occultation measurements were not carried out between 1980 and 1998. Later, the MGS observed 5600 electron density profiles from this experiment during 24 December 1998 to 9 June 2005 [Withers *et al.*, 2008]. The radio occultation experiment was also onboard Mars Express (MEX) and has measured 500 electron density profiles [Haider and Mahajan, 2014]. These profiles show *E* and *F* peaks at altitudes of ~115 km and 135 km due to absorption of X-ray (10–90 Å) and solar EUV (90–1025 Å) radiations, respectively. In addition to the radio occultation experiment, the MEX also carried the Mars Advanced Radar for the Subsurface and Ionosphere Sounding (MARSIS) experiment that measured electron density profiles above the *F* peak. There are no measurements in the *D* region ionosphere of Mars [Haider *et al.*, 2012].

Responses to X-ray flares in the Martian ionosphere were first reported by Mendillo *et al.* [2006] who analyzed two flares that occurred on 15 and 26 April 2001. They found ~200% enhancement in electron density in the *E* region ionosphere due to the effect of these flares. Later, Haider *et al.* [2009] studied the response to the solar X-ray flare of 13 May 2005 in the Martian ionosphere. This flare caused enhancement in the *E* region ionosphere by factors of 6 to 10. A response to coronal mass ejection (CME) was also observed at Mars after ~38 h when the CME encountered the GOES and deposited energy in the *E* region ionosphere. Mahajan *et al.* [2009] reported effects of seven X-ray flares in the Martian ionosphere that occurred on 24 November 2000; 2, 10, and 15 April 2001; 29 and 31 May 2003; and 13 May 2005. Their analysis have shown three major results: (1) X-ray flares produced a well-defined *E* layer peak, not always seen in the Martian ionosphere on other days; (2) some X-ray flares affected both the *E* and *F* layers of the Martian ionosphere; and (3) the enhanced *E* peaks can be formed due to photon fluxes of wavelength range of 10–13 nm. The extension of flare effect can also be found in the *F* layer due to hardening of the 26–91 nm spectral band as measured by Solar EUV Monitor on Solar Heliospheric Observatory. Lollo *et al.* [2012] also studied ionospheric responses to the X-ray flares of 15 and 26 April 2001. They reported that the *E*-peak electron density can exceed that of the *F*-peak during intense solar flares. Haider *et al.* [2012] modeled the effects of solar X-ray flares measured by GOES 12 in the *E* region ionosphere of Mars during the periods 29 May to 3 June 2003, 15–20 January 2005, and 12–18 May 2005. They investigated ionospheric responses to solar X-ray flares and CME that occurred within these intervals. A large increase in electron density, by factors of 5–8, was obtained by their model in the *E* region ionosphere of Mars due to solar X-ray flares that occurred on 29 May 2003, 31 May 2003, 17 January 2005, and 13 May 2005. They also identified shock-triggered enhancements, where electron densities in the *E* region ionosphere increased by a factor of 2 during 30–31 May 2003, 2–3 June 2003, and 16–17

May 2005. Recently, *Fallows et al.* [2015] developed a response function to study the change in electron density due to solar X-ray flares. This function can be used to predict electron density enhancements due to solar flare or to estimate the strength of a solar flare which has impacted the Mars ionosphere. Using the response function they confirmed the earlier findings of *Mendillo et al.* [2006] and *Mahajan et al.* [2009] that the relative enhancements in the electron density caused by solar flares increase with increasing intensity of the solar flare. The MARSIS experiment also measured an increase in the peak electron density of about 30% during a solar flare, which returned to the preflare level within a few minutes [*Nielsen et al.*, 2006]. The response of this flare in the *F* region was smaller than that observed in the *E* region, and therefore, it was not detected by radio occultation observations.

In this paper we have studied six new electron density profiles obtained from MGS that we have found as carrying signatures of a solar flare response in the *E* region ionosphere of Mars. These profiles were obtained on 6 days: 28 March and 6 April 2001, 17 and 18 March and 21 April 2003, and 19 February 2005 (these dates have been identified previously by *Fallows et al.* [2015] for possible detections of a flare response in the Martian ionosphere). A time series of photoionization and photoelectron impact ionization rates, photoelectron flux, ion/electron density, and ionospheric electron content (IEC) are also estimated using a time-dependent Analytical Yield Spectrum (AYS) method for each flare day between 00:00 to 24:00 UT at high solar zenith angles (SZAs) (71° – 73°) in the *E* region ionosphere. We have found that the ion production rates, photoelectron flux, and ion and electron densities increased by 1–2 orders of magnitude at the peak of X-ray flares. The estimated IEC values were compared with the IEC obtained from the measured *E* region electron density profiles. We report that the normalized IEC of the simulated *E* layer increased by factors of 5–10 at the peak flare time compared to a factor of ~ 2 enhancements in the normalized IEC of the corresponding MGS profile, measured at variable times after the peak flare.

2. Objectives

The three main points/objectives focused in this paper are as follows:

1. The solar flare response is a key problem in the planetary ionospheres. In the past effects of several solar flares have been observed on Mars' ionosphere. In this paper we have studied Martian *E* region ionospheric response to six new X-ray flares that occurred on 28 March and 6 April 2001, 17 and 18 March and 21 April 2003, and 19 February, 2005.
2. We have developed a time-dependent model for the photoionization and photoelectron impact ionization rates, photoelectron flux, ion/electron density, and IEC due to X-ray ionizations in the Martian ionosphere. This model is tested for six X-ray flare measurements (listed in item 1 above).
3. Very little is known about the X-ray aeronomy on Mars during the flare events. The production rates, photoelectron flux, ion/electron density, and IEC produced by X-rays are very much different in the *E* region from the *F* region ionosphere. Our model describes the aeronomy of Mars in the *E* region ionosphere for the X-ray flare condition.

3. Motivation

There are extensive literatures on the effects of solar X-ray flares in the Earth's ionosphere [*viz.* *Rastogi et al.*, 1999; *Thomson et al.*, 2004; *Xiong et al.*, 2011; *Qian et al.*, 2012; *Sripathi et al.*, 2013; *Nogueira et al.*, 2015]. However, very little is known about aeronomy due to the effect of solar flare in the Martian ionosphere. In this paper we have attempted to make a comprehensive exposition of basic processes involved in the aeronomy of Mars for the *E* region ionosphere during solar flares. Accordingly, we have obtained a balance between general description of different phenomena in terms of modeling and actual observation. We have calculated time series of photoionization rates, photoelectron impact ionization rates, photoelectron flux, ion density, electron density, and IEC due to effect of six X-ray flares in the *E* region ionosphere of Mars. The calculated IEC are compared with the measured IEC. It has been our goal to emphasize the fundamental character of the *E* region ionosphere of Mars without detailed descriptions of global morphology. Consequently, considerable discussion has been given to production rates, photoelectron flux, plasma density, and chemical reactions and to different collisional interactions involving X-ray radiation.

Bougher et al. [2001] modeled the MGS electron density profiles in the daytime ionosphere by using a Mars Thermosphere General Circulation Model for MGS condition. They found *E* peak electron density

smaller by a factor of 10 than the measurements. Therefore, they increased standard solar X-ray fluxes (18–50 Å) by a factor of 10 in their model to produce *E* layer electron density profiles for comparison with MGS observations. Later Fox [2004] constructed standard models by adopting the SC#21REFW and F79050N solar fluxes [Torr and Torr, 1979] for the calculation of photoionization rate, photoelectron impact ionization rate, ion density, and electron density in the daytime ionosphere of Mars at low and high solar activity periods, respectively. They did not model the MGS electron density profiles observed at flare time. However, they argued that increasing the solar X-ray flux by a uniform factor cannot reproduce the *E* peaks that have been observed in most of the electron density profiles by the MGS. Recently, Lollo *et al.* [2012] developed a one-dimensional ionosphere model for the calculation of electron density profiles, which were compared with the MGS observations during the X-ray flares of 15 and 26 April 2001. They assumed a neutral model atmosphere, which was required to reproduce the electron density profiles observed by MGS during these flares. Using this model they predicted that the peak electron density in the *E* region can exceed from the *F* region ionosphere for a short period during intense flare time. Thus, the ionospheric predictions of *E* region ionosphere are not perfectly consistent with the MGS observations. Therefore, an accurate representation of physical and chemical models in the *E* region ionosphere of Mars is required for flare conditions. The simulation presented in this paper calculates photoionization rates, photoelectron impact ionization rates, photoelectron flux, ion density, electron density, and IEC simultaneously in the *E* region ionosphere of Mars due to effect of solar X-ray flares. Our simulations are most consistent with the MGS observations for flare conditions.

For the first time, we have developed a time-dependent AYS model of ionization to study the ionospheric response of a solar X-ray flare that can be modeled in time throughout the flare event. This model has been found very useful to study the X-ray aeronomy in the *E* region ionosphere of Mars. The calculations based on AYS model are simpler to carry out as compared to those by other methods such as two-stream [Nagy and Banks, 1970; Haider *et al.*, 1992], Boltzmann transport [Mantas and Hanson, 1987], Monte Carlo [Kallio and Barabash, 2001; Haider *et al.*, 2002], and hybrid and magnetohydrodynamic models [Nagy *et al.*, 2004; Ma *et al.*, 2008; Kallio *et al.*, 2010]. However, simplicity of this model is not at the cost of accuracy of the results [Singhal and Haider, 1984]. The ease of the use of this model has been clearly demonstrated in the present simultaneous calculations of time-dependent photoionization rates, photoelectron impact ionization rates, photoelectron flux, ion density, electron density, and IEC in the *E* region ionosphere of Mars. This model is based upon the sets of several atmospheric parameters like solar spectrum, neutral densities, plasma temperature, elastic and inelastic cross sections, photoabsorption, and photoionization cross sections. Such an approach is unique and involves the large number of calculations that have gone into preparation of results presented in this paper. The model sensitivity/uncertainty is given in section 8.

4. Solar X-ray Flare Observations

Several solar flares have been observed from Geostationary Operational Environmental Satellite (GOES), which are measuring solar fluxes at smaller wavelength bands from 0.5 to 3 Å and 1 to 8 Å [Bornmann *et al.*, 1996]. Figures 1a–1f represent a time series of solar X-ray flux distributions that were observed by GOES 10 on the selected days. These observations show a greater enhancements in the wavelength bands 0.5–3 Å and 1–8 Å, which can increase electron densities in the *E* region ionosphere of Mars. The dashed vertical lines in Figures 1a–1f represent the flare time when electron density profiles on Mars were measured by the MGS.

The solar soft X-ray varies between wavelengths 1 and 90 Å [Haider *et al.*, 2011; Haider and Mahajan, 2014]. The *E* layer is mostly formed at about 112–115 km due to ionization produced by X-ray flux in the wavelength range of 18 to 50 Å [cf. Martinis *et al.*, 2003; Fox, 2004; Haider *et al.*, 2002]. There are no measurements of X-ray fluxes at this wavelength region during the flare period. GOES measured X-ray fluxes at shorter wavelength range of 1–8 Å during the flare events. The solar fluxes for X-ray flares at wavelengths ≤ 10 Å will be attenuated at lower altitude and can contribute more to the *E* region ionization. Haider *et al.* [2002] found that X-ray fluxes at wavelengths ≥ 10 Å contributed smaller to the *E* region ionization by about an order of magnitude in comparison to the ionization produced by X-ray fluxes at shorter wavelength range (1–8 Å) during the flare period. This is consistent with the results predicted by Lollo *et al.* [2012] in the *E* region ionosphere of Mars for flare condition. Therefore, we have used GOES 1–8 Å flux in our model calculation.

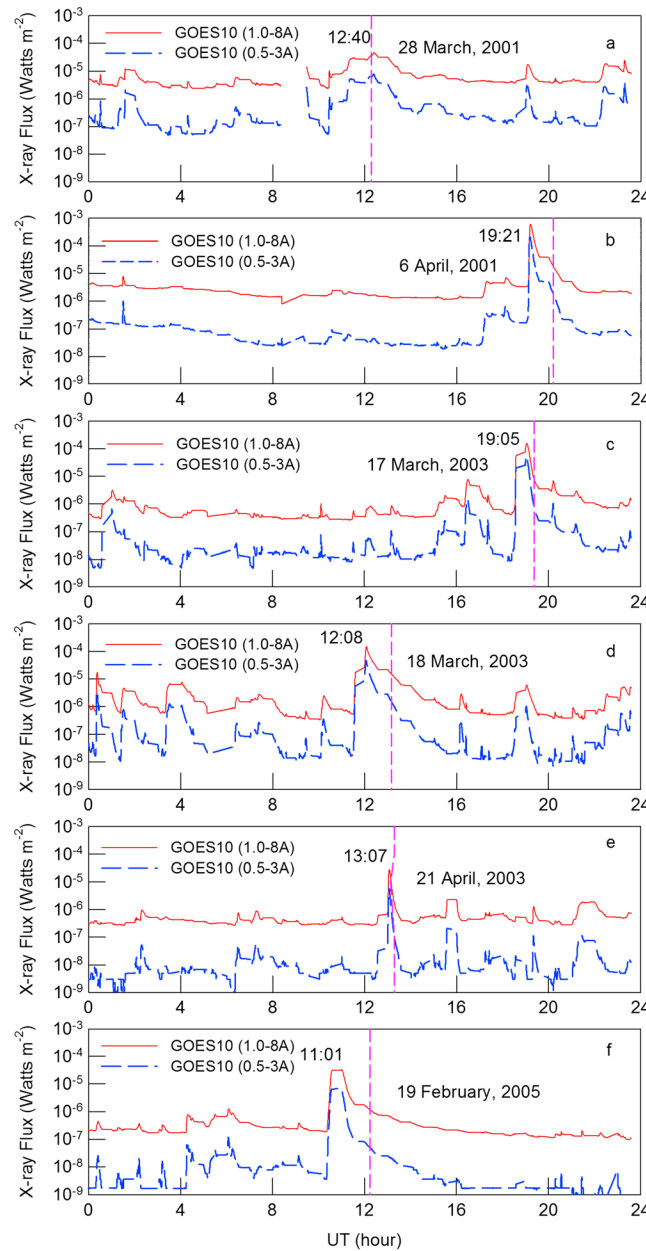


Figure 1. Time series of solar X-ray photon fluxes for (a and b) 28 March and 6 April 2001, (c–e) 17 and 18 March and 21 April 2003, and (f) 19 February 2005 as observed by GOES 10. The dashed vertical lines in each panel represent flare time when electron densities were measured by MGS on Mars.

There are nine electron density profiles, which did not show *E* peaks clearly. These profiles are integrated from their lower altitude to 120 km (the IEC values are not changing significantly if the upper limit of the integration is changed between 105 km and 120 km). All these profiles were observed at high latitudes and high SZA. About 3% error is found in these observations [Hinson et al., 1999]. Mendillo et al. [2006] have reported about 10–15% day-to-day and longitudinal variability in the *E* layer peak.

We have plotted all the profiles in Figures 2a–2f (left column) for each flare day. In these figures, lines marked with stars (red) represent flare-time electron density profiles and the thin solid lines (black) represent profiles observed at other times on the respective day. Universal times (UT), local times (LT), SZA, and latitudes for these profiles are also shown in each figure. It can be noted that the electron densities were enhanced in the *E* region ionosphere during these flares. These effects can be understood more clearly in Figures 2a–2f

5. Response of Mars Ionosphere to Solar Flares

The MGS data set is the largest and has highest cadence in observations during solar maximum condition at Mars. Therefore, it is best suited to study the effects of solar flares on Martian ionosphere. At 2 h cadence the effects of a solar flare are found to be visible in only a single profile. However, several additional profiles are available within 2 h at the flare peak for comparison of the flare affected profiles. In Figures 2a–2f we have plotted 52 electron density profiles with apparent solar flare responses in six profiles on 28 March and 6 April 2001, 17 and 18 March and 21 April 2003, and 19 February 2005 at 12:28, 20:13, 19:38, 13:17, 13:17, and 12:24 UT, respectively (the flare profiles were observed at high latitudes with the coordinates given by (85.4°N, 207.2°E), (84.8°N, 252.5°E), (82.0°N, 315.7°E), (81.7°N, 58.6°E), (74.8°N, 48.6°E), and (79.5°N, 349.3°E), respectively). In these figures most of the plasma resides in the *F* region at about 140 km, where neutral atmosphere molecules are ionized by EUV radiation [Fox and Yeager, 2006]. Below this region the *E* layer is formed where soft X-ray photons ionize the neutral molecules. The *E* layer does not represent always a clear peak. Out of 52 electron density profiles, 10 profiles showed a clear peak at altitudes 105 to 110 km, 18 profiles at altitudes 110 to 115 km, and 15 profiles at altitudes 115 to 120 km. We have integrated these profiles from their lowest height to *E-F* valley altitudes to obtain the IEC in the *E* region ionosphere.

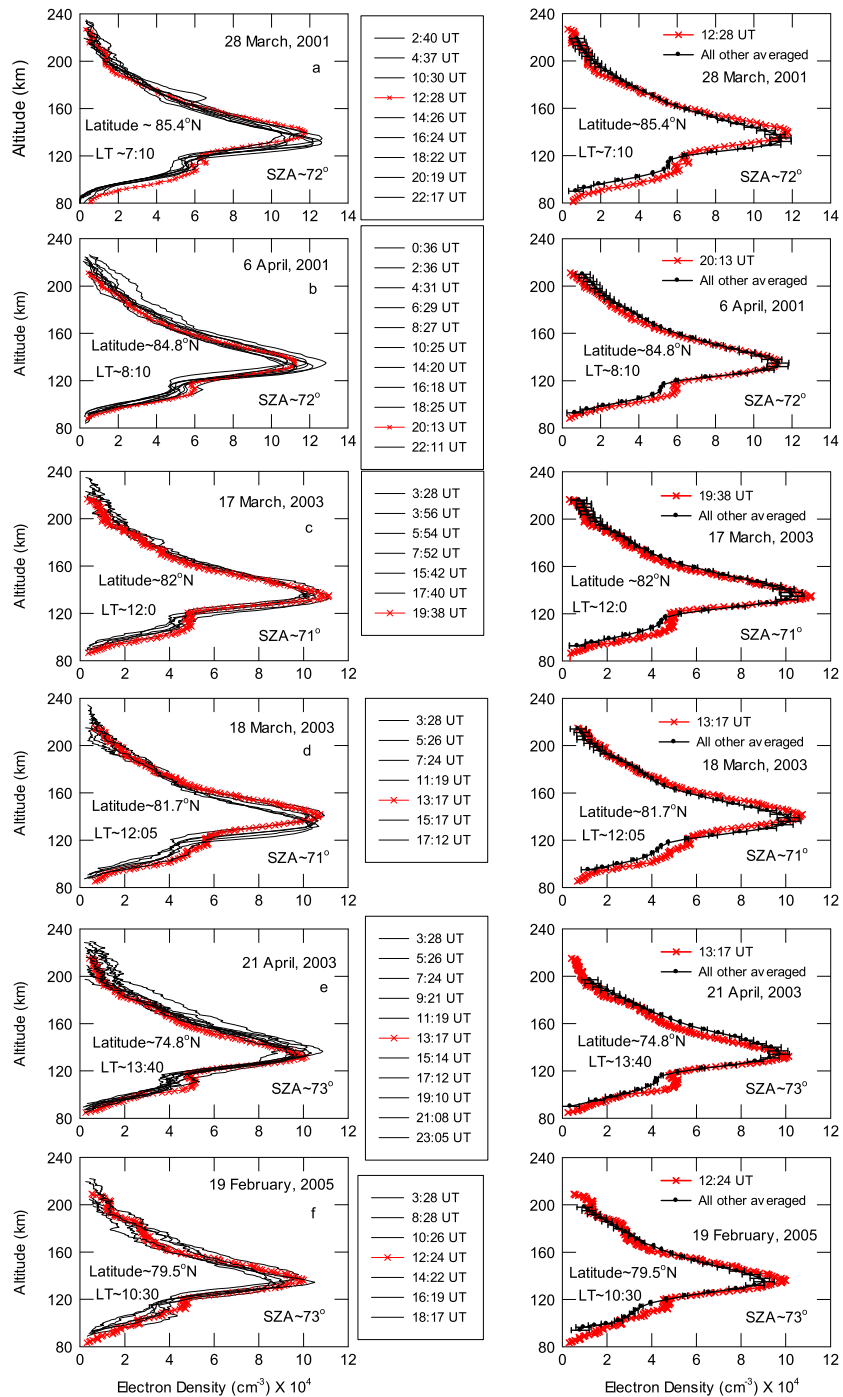


Figure 2. (a–f, left) Electron density profiles observed by MGS on each of six flare days. Flare profiles are plotted by red lines with star. (a–f, right) Flare time profile is compared with the average of nonflare profiles for the respective day. The standard deviation bars are also plotted over averaged nonflare profiles. The latitude, LT, and SZA refer to the flare time.

(right column), where flare-induced profiles are compared with the average of nonflare profiles for the respective day. The standard deviation bars are plotted over averaged nonflare profiles. We report that the flare time profiles were observed mostly during the decay phase of the solar X-ray fluxes of those flares. The flare-time profiles on 6 April 2001, 17 March 2003, 21 April 2003, and 19 February 2005 represent a well-developed *E* peak at about 115 km. The *E* layer peak is not always seen in the other flare and nonflare profiles. The electron density profiles on 28 March 2001 and 6 April 2001 were recorded when X-ray fluxes

Table 1. Characteristics of Solar X-ray Flares and Affected MGS Electron Density Profiles

| Date | Start Time (UT) | Peak Time(UT) | End Time (UT) | Flare (Class) | Location (Sun Disc) | Region | MGS ProfileNo. | MGS Flare ProfileNo. | ESM | SZA |
|-----------|-----------------|---------------|---------------|---------------|---------------------|--------|----------------|----------------------|-------|-----|
| 28/3/2001 | 11:21 | 12:40 | 13:06 | M 4.3 | N17E11 | 9393 | 9 | 1087Q29A | 34.6° | 72° |
| 6/4/2001 | 19:10 | 19:21 | 19:31 | X 5.6 | S21E47 | 9415 | 11 | 1096U17A | 30.2° | 72° |
| 17/3/2003 | 18:50 | 19:05 | 19:16 | X 1.5 | S14W26 | 0314 | 7 | 3076T44A | 62.3° | 71° |
| 18/3/2003 | 11:51 | 12:08 | 12:20 | X 1.5 | S16W39 | 0314 | 7 | 3077N24A | 61.7° | 71° |
| 21/4/2003 | 12:54 | 13:07 | 13:14 | M 2.8 | N18E09 | 0338 | 11 | 3111N21A | 46.3° | 73° |
| 19/2/2005 | 10:36 | 11:01 | 11:13 | M 3.3 | S09W32 | 0732 | 7 | 5050M3FA | 97.2° | 73° |

were quite high. Therefore, the flare effects in the *E* layers are quite prominent for these particular events. In Figure 2b (left column) the *E* layer peak value at 22:11 UT is larger at altitude 113 km by ~5–10% than the peak flare profile at 20:13 UT. However, the average of nonflare profiles of *E* region does not increase from the flare profile on this date. Therefore, the enhancement in the peak electron density at 22:11 UT may be associated with postflare effect on 6 April 2001. Thus, the effects of X-ray flares are found to be visible in some cases during 2–3 h cadence period. Supporting information for selected X-ray flares and MGS flare profiles are given in Table 1.

6. Modeling of the X-ray Ionization on Mars

We have calculated temporal variability of photoionization rate, photoelectron impact ionization rate, photoelectron flux, electron density, and IEC using time-dependent AYS method for X-ray ionization on Mars. This method is based on Monte Carlo approach. Initially, X-ray radiation is introduced in the Martian atmosphere at solar zenith angle χ and time t . Later, the energy of photoelectrons and their positions were calculated. In this method the elastic and inelastic collisions are included between photoelectrons and neutral species and photoelectron-photoelectron Coulomb collision. The scattering due to photoelectron-ion interaction is neglected. The photoelectrons are produced in the Martian atmosphere at time t , solar zenith angle χ , and some pitch angles. We have generated a real number between 0 and 1 from a random generator. It determined whether a collision took place or not. The Coulomb losses were calculated from Butler-Buckingham formula [Dalgarno *et al.*, 1963]. The elastic and inelastic scattering calculations are carried out by Porter and Jump [1978] method and Jackman *et al.* [1977] method, respectively. It is assumed that photoelectrons are ejected isotropically. We have used mixture of five gases CO₂, N₂, O₂, O, and CO in the AYS model at altitude h and time t . This method has been used by us in several research problems related to electron energy degradation in planetary atmospheres [Green *et al.*, 1977; Singhal *et al.*, 1980; Singhal and Green, 1981; Haider and Singhal, 1983; Singhal and Haider, 1984; Seth *et al.*, 2002, 2006; Bhardwaj and Jain, 2009; Haider *et al.*, 2010; Pandya and Haider, 2014].

Recently, Pandya and Haider [2014] used the AYS method to calculate the altitude profile of electron density due to impact of meteoroids, solar X-ray, and EUV radiation in the dayside atmosphere of Mars. We have now extended this method by including a time variable to study the temporal variability in the *E* region ionosphere of Mars. This method calculates photoionization and photoelectron impact ionization rates, photoelectron flux, ion/electron density, and IEC simultaneously at different height, time, and energy. Following Pandya and Haider [2014] the analytical form of the AYS method is represented by

$$U(E, E_0) = C_0 + C_1 X + C_2 X^2 \tag{1}$$

$$X = \frac{(E_0/1000)^{0.585}}{E + 1} \tag{2}$$

where C_0 , C_1 , and C_2 are adjustable parameters of CO₂, N₂, O₂, O, and CO. These parameters were obtained by a nonlinear least squares fitting procedure [Singhal and Green, 1981]. The parameters C_0 , C_1 , and C_2 do not depend on time because it embodies the nontime variable information of the degradation process. The first term of equation (1) arises from primaries, while the second and third terms are produced from secondary and tertiary generations of the electron collisions respectively. The $U(E, E_0)$ is defined as $N(E)/\Delta(E)$ [Green *et al.*, 1977], where $N(E)$ is the number of electrons in the bin centered at energy E after one bin has been emptied and before the next lower nonempty bin of width $\Delta(E)$ centered at E is considered. In this approach the energy range between initial values and threshold of the state is divided into bins. The

equation (1) calculates yield of a single gas in the Martian atmosphere. The composite yield spectrum for a mixture of gas i is obtained at time t by weighting the component of yield spectrum as given below:

$$U^c(E, t, E_o) = \sum_i f_i(t) U_i(E, E_o) \quad (3)$$

The value of f_i is a fractional composition and is related to time t as

$$f_i(t) = \frac{S_i n_i(h, t)}{\sum_j S_j n_j(h, t)} \quad (4)$$

where S_i/S_j is the average value of $\sigma_{Ti}(E)/\sigma_{Tj}(E)$ between $E_{\min} = 2$ eV to E_o , $\sigma_{Ti}(E)$ is the total (elastic + inelastic) cross sections of i th gas, and $n_i(h, t)$ is the neutral density at altitude h and time t . The neutral densities of CO_2 , N_2 , O_2 , O , and CO are taken from Mars Climate Database (MCD) model for six flare days at different time and locations of MGS observations [Millour et al., 2014]. The time-dependent photoelectron impact ionization rates are calculated as given below:

$$J(h, \chi, t) = \int_{W_i}^{\infty} dE_o \int_E^{\infty} P_i(E, t) Q(h, \chi, E, t) U^c(E, E_o, t) dE \quad (5)$$

where $J(h, \chi, t)$ is the photoelectron production rate at altitude h , solar zenith angle χ , and time t ; $Q(h, \chi, E, t)$ is the primary photoelectron production rate; W_i is the threshold energy for ionization of gas i ; and $P_i(E, t)$ is the ionization probability as given below:

$$P_i(E, t) = \frac{n_i(h, t) \sigma_i(E)}{\sum_j n_j(h, t) \sigma_j(E)} \quad (6)$$

Here σ_i is the photoelectron impact ionization cross sections of CO_2^+ , N_2^+ , O_2^+ , O^+ , and CO^+ , which are taken from Josphipura et al. [2007, 2009]. The primary photoelectron energy spectrum $Q(h, \chi, E, t)$ is calculated as given below:

$$Q(h, \chi, E, t) = \sum_i n_i(h, t) \sum_{\lambda} \sigma_i^l(\lambda) I(\infty, \lambda, t) \delta\left(\frac{hc}{\lambda} - E - W_i\right) \exp\left[-\sum_i \sigma_i^A(\lambda) \int_h^{\infty} n_i(h, t) \text{Ch}(X, \chi) dh\right] \quad (7)$$

where $\sigma_i^l(\lambda)$ and $\sigma_i^A(\lambda)$ are respectively the photoionization and photoabsorption cross sections at wavelength λ , $I(\infty, \lambda, t)$ is the incident X-ray photon flux at time t , and $\delta\left(\frac{hc}{\lambda} - E - W_i\right)$ is the delta function, in which $\frac{hc}{\lambda}$ is incident photon energy and E is the energy of ejected photoelectrons. The term $\text{Ch}(X, \chi)$ is the Chapman function for grazing incidence [Smith and Smith, 1972], which is used to calculate the absorption of X-ray radiation obliquely through the atmosphere. Here χ is solar zenith angle and $X = (R_m + h)/H$, where R_m is the radius of Mars and H is scale height of the neutral atmosphere. In equation (7) the incident X-ray photon flux is taken from Figure 1 between wavelength range of 1–8 Å at 5 min time resolution and energy bins of 0.2 Å. The photoabsorption and photoionization cross sections of CO_2 , N_2 , O_2 , O , and CO are taken from Pandya and Haider [2014], who compiled it in Tables A1 and A2, respectively, from different investigators [Torr and Torr, 1979; Cairns and Samson, 1965; Cook et al., 1966; Lee et al., 1973; McCulloh, 1973; Iida et al., 1986; Watanabe et al., 1967]. The photoionization rate $Q(h, \chi, t)$ is obtained from primary photoelectron spectrum $Q(h, \chi, E, t)$ by integrating it over energy E . The time-dependent photoionization and photoelectron impact ionization rates are calculated for six flare days on 28 March and 6 April 2001, 17 and 18 March and 21 April 2003, and 19 February 2005 at solar zenith angles 72°, 72°, 71°, 71°, 73°, and 73° respectively. The general expression for photoelectron production rate is given below:

$$J(h, \chi, t) = n_i(h, t) \int_{W_i}^{\infty} \phi(h, \chi, E, t) \sigma_i(E) dE \quad (8)$$

Comparing equations (5) and (8) we can obtain expression for photoelectron flux as given below:

$$\phi(h, \chi, E, t) = \int_E^{\infty} \frac{Q(h, \chi, E, t) U^c(E, E_o, t)}{\sum_j n_j(h, t) \sigma_j(E)} dE_o \quad (9)$$

Table 2. Chemical Reactions

| Reaction | Rate Coefficient (cm^3s^{-1}) | Reference |
|--|---|--------------------------------|
| $\text{N}_2^+ + \text{CO}_2 \rightarrow^{k_1} \text{CO}_2^+ + \text{N}_2$ | $k_1 = 7.7 \times 10^{-10}$ | Fehsenfeld et al. [1969] |
| $\text{N}_2^+ + \text{O} \rightarrow^{k_2} \text{NO}^+ + \text{N}$ | $k_2 = 1.3 \times 10^{-10}$ | Fehsenfeld et al. [1970] |
| $\text{N}_2^+ + \text{CO} \rightarrow^{k_3} \text{CO}^+ + \text{N}_2$ | $k_3 = 7.4 \times 10^{-11}$ | Ikezoe et al. [1986] |
| $\text{N}_2^+ + \text{NO} \rightarrow^{k_4} \text{NO}^+ + \text{N}_2$ | $k_4 = 3.3 \times 10^{-10}$ | Fehsenfeld et al. [1970] |
| $\text{N}_2^+ + \text{e}^- \rightarrow^{k_5} \text{N} + \text{N}$ | $k_5 = 3.0 \times 10^{-7} \times (300/T_e)^{1/3}$ | Frommhold and Biondi [1967] |
| $\text{N}_2^+ + \text{O}_2 \rightarrow^{k_6} \text{O}_2^+ + \text{N}_2$ | $k_6 = 5.0 \times 10^{-11}$ | Golden et al. [1968] |
| $\text{CO}_2^+ + \text{O} \rightarrow^{k_7} \text{O}^+ + \text{CO}_2$ | $k_7 = 9.6 \times 10^{-11}$ | Fehsenfeld et al. [1970] |
| $\text{CO}_2^+ + \text{O} \rightarrow^{k_8} \text{O}_2^+ + \text{CO}$ | $k_8 = 1.64 \times 10^{-11}$ | Fehsenfeld et al. [1970] |
| $\text{CO}_2^+ + \text{O}_2 \rightarrow^{k_9} \text{O}_2^+ + \text{CO}_2$ | $k_9 = 5.0 \times 10^{-11}$ | Fehsenfeld et al. [1970] |
| $\text{CO}_2^+ + \text{NO} \rightarrow^{k_{10}} \text{NO}^+ + \text{CO}_2$ | $k_{10} = 1.2 \times 10^{-10}$ | Fehsenfeld et al. [1970] |
| $\text{CO}_2^+ + \text{e}^- \rightarrow^{k_{11}} \text{CO} + \text{O}$ | $k_{11} = 1.14 \times 10^{-04} \times (T_e)^{-1}$ | Bauer [1973] |
| $\text{CO}^+ + \text{CO}_2 \rightarrow^{k_{12}} \text{CO}_2^+ + \text{CO}$ | $k_{12} = 1.0 \times 10^{-09}$ | Anicich and Huntress [1986] |
| $\text{CO}^+ + \text{O} \rightarrow^{k_{13}} \text{O}^+ + \text{CO}$ | $k_{13} = 1.4 \times 10^{-10}$ | Anicich and Huntress [1986] |
| $\text{CO}^+ + \text{NO} \rightarrow^{k_{14}} \text{NO}^+ + \text{CO}$ | $k_{14} = 3.30 \times 10^{-10}$ | Fehsenfeld and Ferguson [1972] |
| $\text{CO}^+ + \text{e}^- \rightarrow^{k_{15}} \text{O} + \text{C}$ | $k_{15} = 2.7 \times 10^{-7} \times (300/T_e)^{0.5}$ | Fehsenfeld and Ferguson [1972] |
| $\text{O}^+ + \text{NO} \rightarrow^{k_{16}} \text{NO}^+ + \text{O}$ | $k_{16} = 1.0 \times 10^{-11}$ | McFarland et al. [1974] |
| $\text{O}^+ + \text{O}_2 \rightarrow^{k_{17}} \text{O}_2^+ + \text{O}$ | $k_{17} = 2.0 \times 10^{-11} \times (300/T_n)^{0.5}$ | Ferguson [1969] |
| $\text{O}^+ + \text{N}_2 \rightarrow^{k_{18}} \text{NO}^+ + \text{N}$ | $k_{18} = 1.2 \times 10^{-12} \times (300/T_n)$ | Ferguson [1967] |
| $\text{O}^+ + \text{CO}_2 \rightarrow^{k_{19}} \text{O}_2^+ + \text{CO}$ | $k_{19} = 1.1 \times 10^{-9}$ | Fehsenfeld et al. [1970] |
| $\text{O}^+ + \text{e}^- \rightarrow^{k_{20}} \text{O}$ | $k_{20} = 3.26 \times 10^{-12} \times (30/T_e)^{0.7}$ | Molina-Cuberos et al. [2002] |
| $\text{O}_2^+ + \text{e}^- \rightarrow^{k_{21}} \text{O} + \text{O}$ | $k_{21} = 8.75 \times 10^{-6} \times (T_e)^{-0.67}$ | Walls and Dunn [1974] |
| $\text{O}_2^+ + \text{NO} \rightarrow^{k_{22}} \text{NO}^+ + \text{O}_2$ | $k_{22} = 6.3 \times 10^{-10}$ | Fehsenfeld et al. [1970] |
| $\text{NO}^+ + \text{e}^- \rightarrow^{k_{23}} \text{N} + \text{O}$ | $k_{23} = 1.08 \times 10^{-7} (1000/T_e)^{1.2}$ | Biondi [1972] |

The photoelectron flux is calculated at time t for energy grids of width 2 eV from 0 to 10 eV and of 2.5 eV between 10 to 1000 eV.

The photoionization and photoelectron impact ionization rates of five ions CO_2^+ , N_2^+ , O_2^+ , O^+ , and CO^+ are added to obtain the total ion production rates, which have been used in the continuity equations. The altitude profiles for the densities of six ions (CO_2^+ , N_2^+ , O_2^+ , O^+ , CO^+ , and NO^+) and electron are calculated at different time under charge neutrality condition by iteration process. In the chemical model the production rate of NO^+ is obtained from the chemical reactions. The production rate of NO^+ is not calculated from the time-dependent AYS method because direct ionization of NO has little effect on the density profile of NO^+ [Fox, 2004]. The neutral density of NO is not given by MCD model. We have taken it from Fox [1993]. It is assumed that the density of NO is not changing significantly with time and locations. The chemical reactions used in our model are given in Table 2. The neutral temperature necessary to calculate the ion and electron densities is taken from the MCD model. The electron temperature is taken from Fox [2009]. The electron density is integrated between altitudes 80 km and 120 km to obtain the IEC in the E region ionosphere. This method is used where the magnetic field is uniform and horizontal in direction. This assumption is appropriate at high latitude of Mars where the magnetic field of solar wind is horizontal in direction such as observed by MGS in the dayside ionosphere [cf. Ness et al., 2000; Haider et al., 2010]. In this case the vertical transport of photoelectrons is inhibited and they lose their energy at the same height where they were produced.

7. Results and Discussion of Model Results: E Region Ionosphere of Mars

Since the distance of Mars from the Sun is greater than that of the Earth from the Sun, the effect of flares in the solar X-ray radiation should be registered on Mars with a longer time delay as compared to that on the Earth. We have calculated the time delay for each flare by dividing the observed distance of the Sun to Mars with the velocity of light. Based on the distance of Mars from the Sun as observed by the MGS [Hinson et al., 1999], the peak solar flux arrived at Mars with a time delay of ~2–5 min after it arrived at Earth. GOES observed the peak X-ray fluxes on 28 March and 6 April 2001, 17 and 18 March and 21 April 2003, and 19 February 2005 at 12:40 UT, 19:21 UT, 19:05 UT, 12:08 UT, 13:07 UT, and 11:01 UT, which are inferred to reach Mars ~5 min later, i.e., 12:45 UT, 19:26 UT, 19:10 UT, 12:13 UT, 13:12 UT, and 11:06 UT respectively. The MGS measured the electron density profiles a few hours before and immediately after the solar flares on each day.

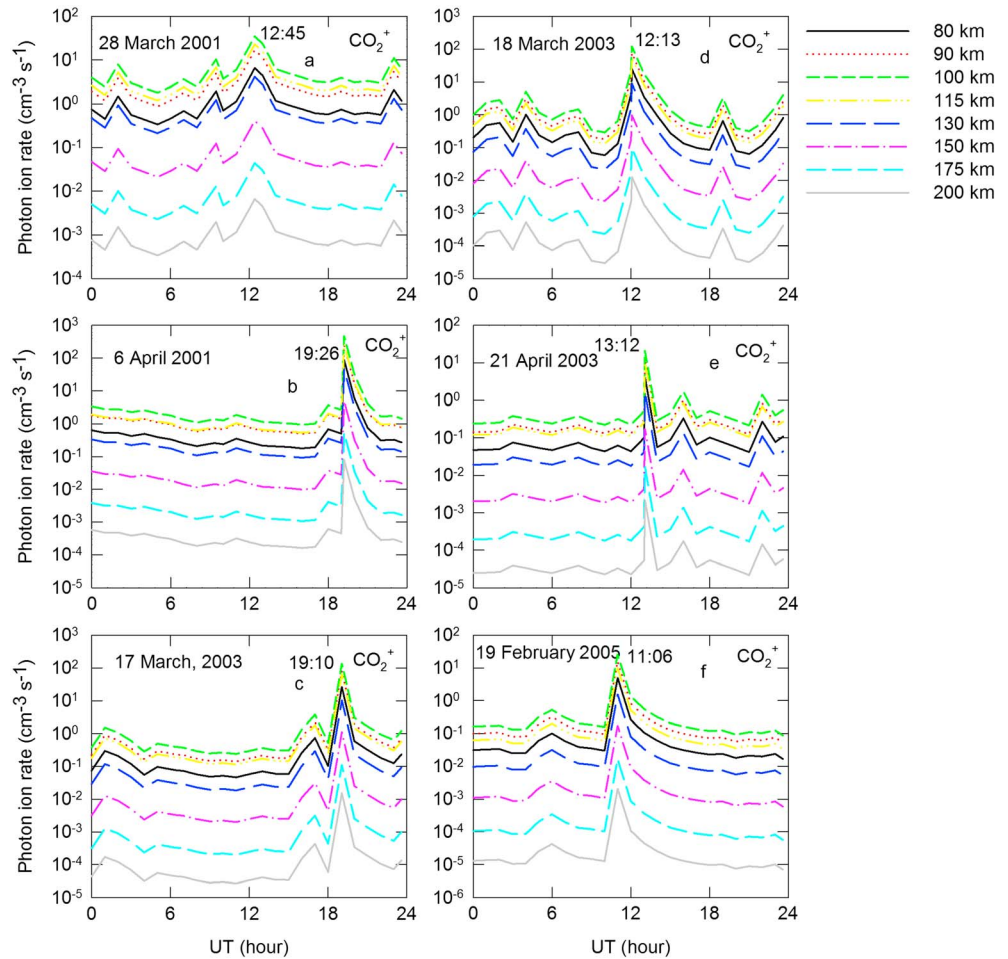


Figure 3. Time series of photoionization rates of CO_2^+ produced by X-ray flares on (a) 28 March 2001, (b) 6 April 2001, (c) 17 March 2003, (d) 18 March 2003, (e) 21 April 2003, and (f) 19 February 2005 in the E region ionosphere of Mars at altitudes 80, 90, 100, 115, 130, 150, 175, and 200 km.

Figures 3a–3f represent a time series of photoionization rates of major ion CO_2^+ at 80, 90, 100, 115, 130, 150, 175, and 200 km due to impact of solar X-ray flares, which occurred on 28 March and 6 April 2001, 17 and 18 March and 21 April 2003, and 19 February 2005 respectively. The photoionization rates produced by X-ray radiation (wavelength band 1–8 Å) peaks at about 100 km in the E region ionosphere of Mars. Due to these flares the peak photoionization rates of CO_2^+ are estimated to be 3.5×10^1 , 4.6×10^2 , 1.3×10^2 , 1.2×10^2 , 2.1×10^1 , and $2.5 \times 10^1 \text{ cm}^{-3} \text{ s}^{-1}$ at flare time 12:45, 19:26, 19:10, 12:13, 13:12, and 11:06 UT, respectively. The photoionization rates increased by 2 orders of magnitudes at the peak X-class flares on 6 April 2001 and 17 and 18 March 2003. These production rates also increased by 1 order of magnitude at the peak M-class flares on 28 March 2001, 21 April 2003, and 19 February 2005. The variations in the photoionization rates after and before the peak flares are also produced each day due to the variations in the X-ray spectrum observed by GOES 10. Figures 4a–4f represent a time series of flare-induced photoelectron impact ionization rates of major ion CO_2^+ at 80, 90, 100, 115, 130, 150, 175, and 200 km. The photoelectron production rates are larger than the photoionization rates. This is because X-ray produces energetic photoelectrons which are attenuated at lower altitude and contribute more to photoelectron impact ionization rates [Haider et al., 2002]. The X-rays have shorter wavelength than the EUV radiation. It does not contribute greatly to photoelectrons which are attenuated at high altitude. The EUV radiation contributes more to photoionization rates than that produced by solar X-rays. The peak photoelectron production rates of CO_2^+ are estimated to be 1.0×10^2 , 2.0×10^3 , 5.5×10^2 , 4.6×10^2 , 8.0×10^2 , and $1.3 \times 10^2 \text{ cm}^{-3} \text{ s}^{-1}$ due to X-ray flares of 28 March and 6 April 2001, 17 and 18 March and 21 April 2003, and 19 February 2005, respectively. We have plotted photoionization and photoelectron

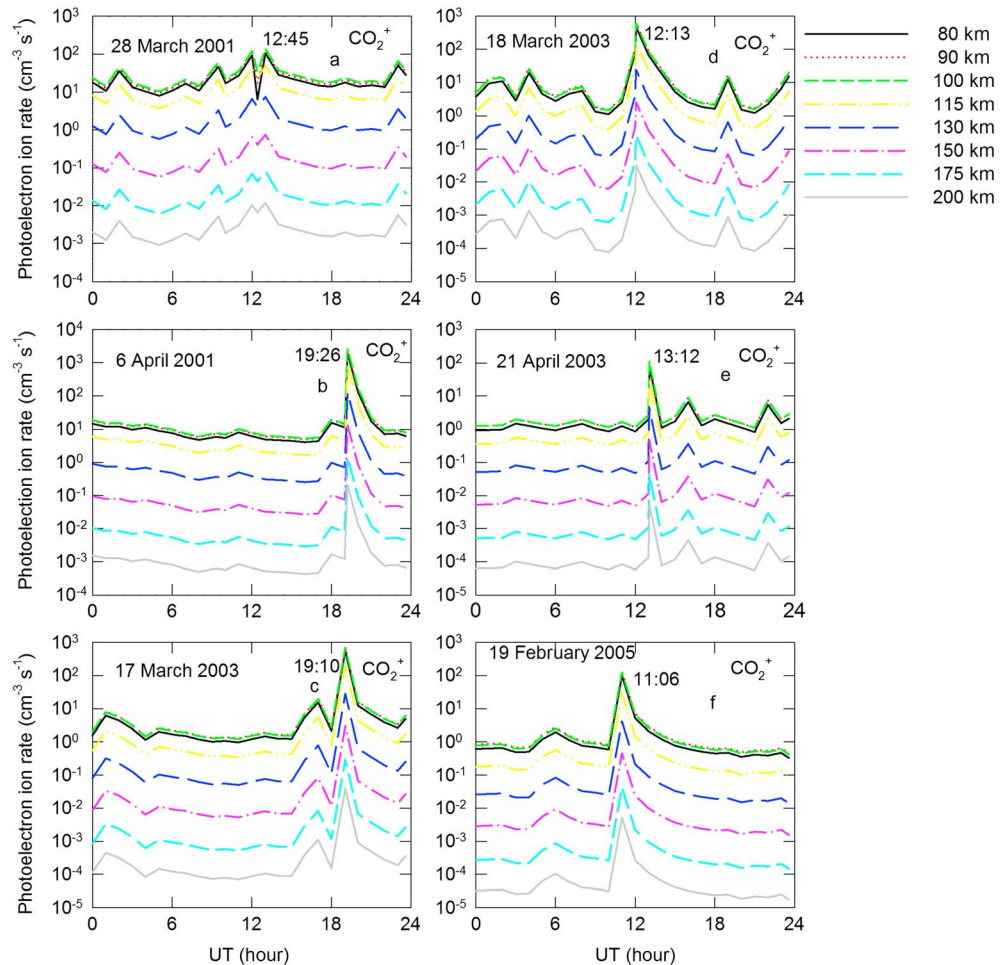


Figure 4. Time series of photoelectron impact ionization rates of CO_2^+ produced by X-ray flares on (a) 28 March 2001, (b) 6 April 2001, (c) 17 March 2003, (d) 18 March 2003, (e) 21 April 2003, and (f) 19 February 2005 in the E region ionosphere of Mars at altitudes 80, 90, 100, 115, 130, 150, 175, and 200 km.

impact ionization rates of CO_2^+ only. The production rates for other ions (N_2^+ , O_2^+ , O^+ , and CO^+) are not plotted because their values are low.

Figures 5a–5f represent an energy distribution of photoelectron fluxes in the E region ionosphere of Mars at peak flare time 12:45, 19:26, 19:10, 12:13, 13:12, and 11:06 UT due to X-ray flares which occurred on 28 March and 6 April 2001, 17 and 18 March and 21 April 2003, and 19 February 2005, respectively. The photoelectron fluxes are decreasing with increasing energy because solar X-ray flux and photoionization cross section are decreasing with increasing energy. As expected a major peak near 25–27 eV is not found in the estimated photoelectron spectra because this peak is produced due to absorption of He II Lyman α at wavelength 304 Å [cf. Haider et al., 2010]. We have used flare-induced X-ray fluxes observed by GOES 10 in the wavelength range 1 to 8 Å for ionization in the E region ionosphere of Mars. The photoelectron spectra are shown between energy 1–1000 eV at altitudes 80, 90, 100, 115, 130, 150, 175, and 200 km. It is found that the photoelectron fluxes are nearly independent of altitude above 115 km because X-ray produces maximum ionization below this altitude. We have also found a small peak at about 200 eV in the photoelectron spectra. This peak can be related to X-ray ionization producing C, N, or O by Auger electrons as reported by Mitchell et al. [2000] in their photoelectron spectra observed by MGS. Figures 6a–6f represent energy distribution of photoelectron fluxes due to X-ray ionizations on 28 March and 6 April 2001, 17 and 18 March and 21 April 2003, and 19 February 2005, respectively, in the absence of flare X-rays (at 0.0 UT), when the ionosphere was quiet. We have compared photoelectron spectra for each day between peak flare time and no flare time. The photoelectron fluxes are larger at the peak flare time by 1–2 orders of magnitude than

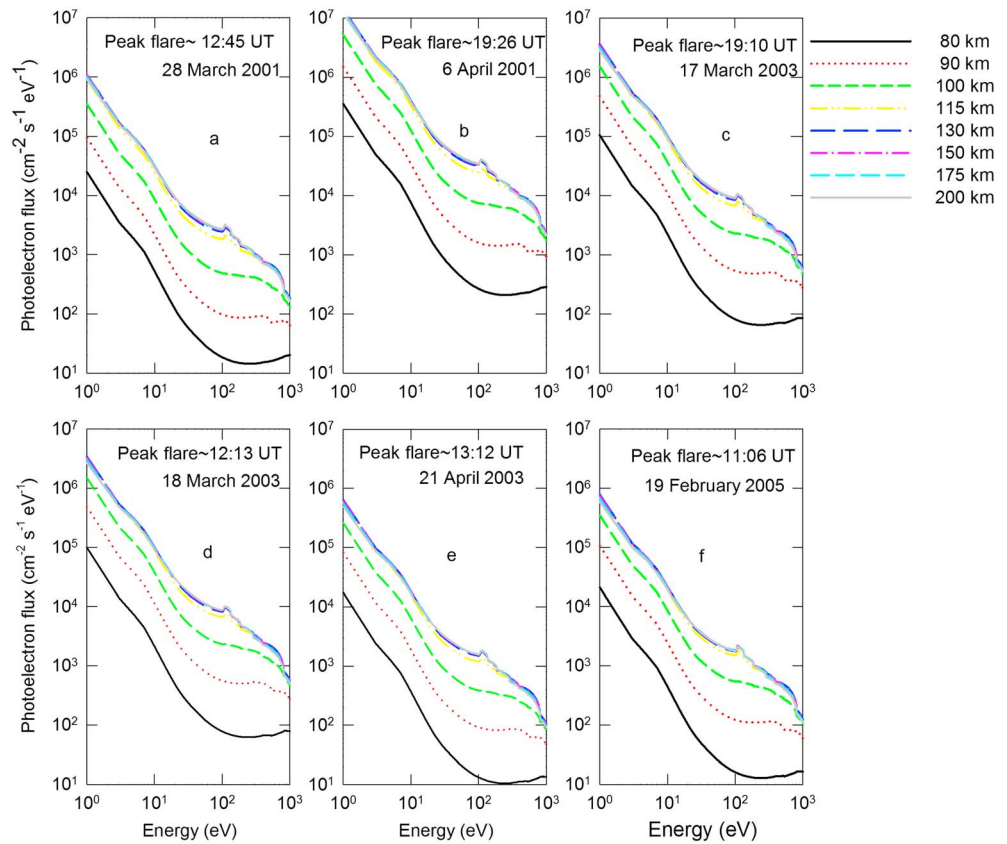


Figure 5. The photoelectron energy fluxes at flare time 12:45, 19:26, 19:10, 12:13, 13:12, and 11:06 UT on (a) 28 March 2001, (b) 6 April 2001, (c) 17 March 2003, (d) 18 March 2003, (e) 21 April 2003, and (f) 19 February 2005, respectively, at altitudes 80, 90, 100, 115, 130, 150, 175, and 200 km.

those estimated at no flare time. In Figures 5b–5d photoelectron fluxes are higher by 2 orders of magnitude due to ionization produced by the peak X-class flares on 6 April 2001 and 17 and 18 March 2003, respectively. In Figures 5a, 5e, and 5f the photoelectron fluxes increased by 1 order of magnitude due to ionization produced by the peak M-class flares on 28 March 2001, 21 April 2003, and 19 February 2005, respectively.

We calculated the flare-induced densities of six ions CO_2^+ , N_2^+ , O_2^+ , O^+ , NO^+ , and CO^+ in the *E* region ionosphere of Mars between altitudes 80 and 200 km. Figures 7a–7f, 8a–8f, and 9a–9f show the temporal variations of ion densities for three major ions NO^+ , CO_2^+ , and O_2^+ , respectively, at altitudes 80, 90, 100, 115, 130, 150, 175, and 200 km due to the six selected X-ray flares, which occurred on 28 March and 6 April 2001 (figures a and b), 17 and 18 March and 21 April 2003 (figures c, d, and e), and 19 February 2005 (figure f). The densities of other ions O^+ , N_2^+ , and CO^+ are not plotted because their values are very low. Initially, the major ion CO_2^+ is produced due to X-ray ionization. Later, it is quickly removed by atomic oxygen and O_2^+ is formed as a dominant ion in the *E* region ionosphere. The second major ion NO^+ is produced in the *E* region due to loss of O_2^+ with NO . The ion NO^+ is fully destroyed by dissociative recombination with electron. The densities of CO_2^+ and O_2^+ are enhanced by 2 orders of magnitude due to the impact of peak X-class flares on 6 April 2001 and 17 and 18 March 2003. These ion densities also increased by 1 order of magnitude due to the impact of peak M-class flares on 28 March 2001, 21 April 2003, and 19 February 2005. In Figures 7a–7f the peak increase of NO^+ due to the flare (from the background) is less than the corresponding peaks of CO_2^+ and O_2^+ because NO^+ is not produced in the ion-neutral model due to primary production source (photoionization rates + photoelectron impact ionization rates). Therefore, X-ray flare produces only a small peak value at about 100 km for the ion density of NO^+ . The densities of NO^+ , CO_2^+ , and O_2^+ are also changing with time on each flare day because of temporal variations in solar X-ray fluxes, neutral densities, and temperatures. The flare-induced peak increase in the NO^+ density are 1.71×10^3 , 1.56×10^3 , 1.75×10^3 , 1.74×10^3 , 1.5×10^3 , and $1.6 \times 10^3 \text{ cm}^{-3}$ at 12:45, 19:26, 19:10, 12:13, 13:12, and 11:06 UT, respectively. In the *E* region ionosphere of Mars the densities of O_2^+ and

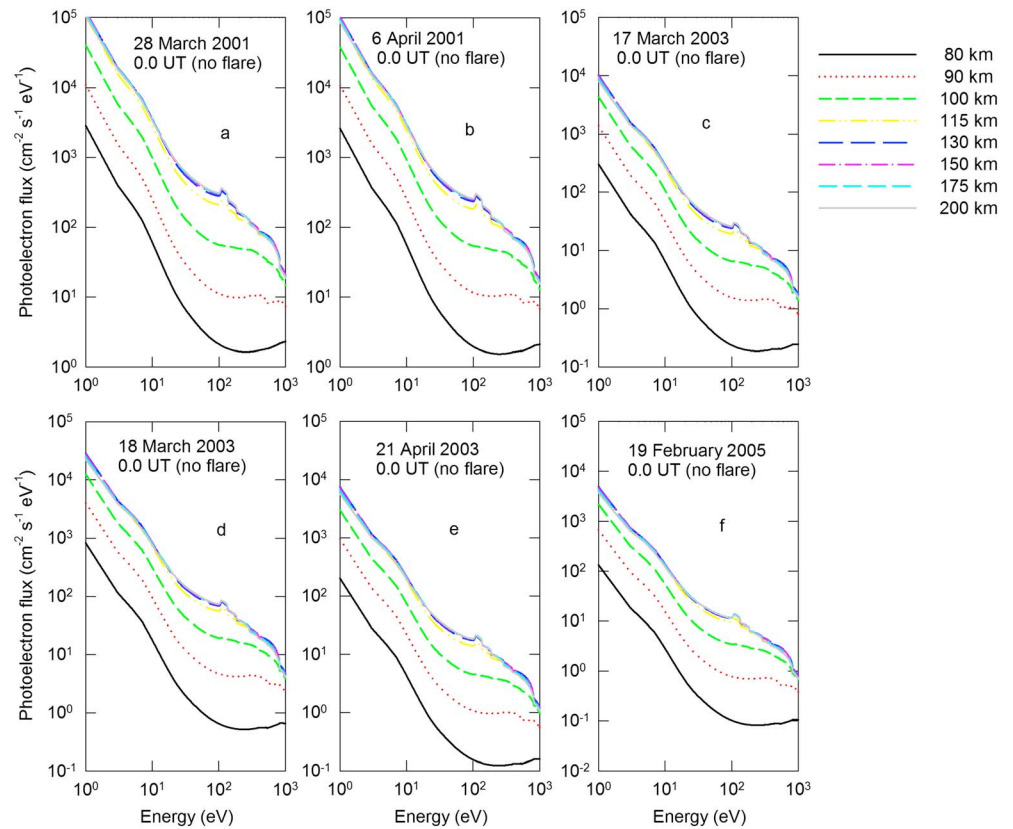


Figure 6. The photoelectron energy fluxes on (a) 28 March 2001, (b) 6 April 2001, (c) 17 March 2003, (d) 18 March 2003, (e) 21 April 2003, and (f) 19 February 2005 for no flare time (0.0 UT) at altitudes 80, 90, 100, 115, 130, 150, 175, and 200 km.

NO^+ are proportional as $[\text{O}_2^+] \propto [\text{CO}_2^+] [\text{O}]/\text{Ne}$ and $[\text{NO}^+] \propto [\text{O}_2^+] [\text{NO}]/\text{Ne}$, respectively, where $[\text{Ne}]$ and $[\text{CO}_2^+]$ are the densities of electron and CO_2^+ , respectively. The peaks of CO_2^+ and O_2^+ are located at about 115 km and 100 km, respectively. The peak ion densities for six selected flares are estimated to be 5.2×10^1 , 6.2×10^2 , 1.2×10^2 , 1.0×10^2 , 3.1×10^1 , and $4.0 \times 10^1 \text{ cm}^{-3}$ for CO_2^+ and 2.0×10^4 , 7.4×10^4 , 3.8×10^4 , 3.5×10^4 , 1.4×10^4 , and $1.5 \times 10^4 \text{ cm}^{-3}$ for O_2^+ at 12:45, 19:26, 19:10, 12:13, 13:12, and 11:06 UT, respectively. The electron density in the E region can be estimated approximately as $\text{Ne} = \sqrt{q/\alpha}$, where q is a sum of photoionization and photoelectron impact ionization rates of CO_2^+ and α is a dissociative recombination rate coefficient equal to $1.9 \times 10^{-7} (300/\text{Te})^{0.5} \text{ cm}^3 \text{ s}^{-1}$ [Mul and McGowan, 1979]. The total production rates (photoionization rates + photoelectron impact ionization rates) of CO_2^+ at the flare peaks are estimated to be 2.6×10^2 , 2.4×10^3 , 8.4×10^2 , 7.6×10^2 , 1.3×10^2 , and $1.6 \times 10^2 \text{ cm}^{-3} \text{ s}^{-1}$ at 12:45, 19:26, 19:10, 12:13, 13:12, and 11:06 UT, respectively. These production rates yield the flare peak electron density $\text{Ne} \sim 1.2 \times 10^4$, 1.0×10^5 , 6.0×10^4 , 6.0×10^4 , 2.4×10^4 , and $2.7 \times 10^4 \text{ cm}^{-3}$ at the flare time 12:45, 19:26, 19:10, 12:13, 13:12, and 11:06 UT, respectively.

Figures 10a–10f represent a time series of electron densities produced by the six selected X-ray flares in the E region ionosphere. The electron densities increased by about an order of magnitude due to the impact of X-class flares on 6 April 2001 and 17 and 18 March 2003, whereas the increases produced by M-class flares on 28 March 2001, 21 April 2003, and 19 February 2005 were smaller. The X-ray ionization produces a broad peak in the electron density profiles at about 100 km. In Figures 2a–2f E region peaks are observed at altitudes 108, 113, 115, 105, 109, and 112 km due to the flares of 28 March and 6 April 2001, 17 and 18 March and 21 April 2003, and 19 February 2005, respectively. Due to these flares the peak electron densities in the E region were observed to be 6×10^4 , 5.8×10^4 , 5×10^4 , 5.5×10^4 , 5.0×10^4 , and $5.2 \times 10^4 \text{ cm}^{-3}$ at 12:28, 20:13, 19:38, 13:17, 13:17, and 12:24 UT, respectively. The peak electron densities for these six selected X-ray flares were estimated to be $\sim 2 \times 10^4$, 7.5×10^4 , 4.0×10^4 , 4.3×10^4 , 1.5×10^4 , and $1.9 \times 10^4 \text{ cm}^{-3}$ at 12:45, 19:26, 19:10, 12:13, 13:12, and 11:06 UT, respectively. The E region peaks are produced due to absorption of

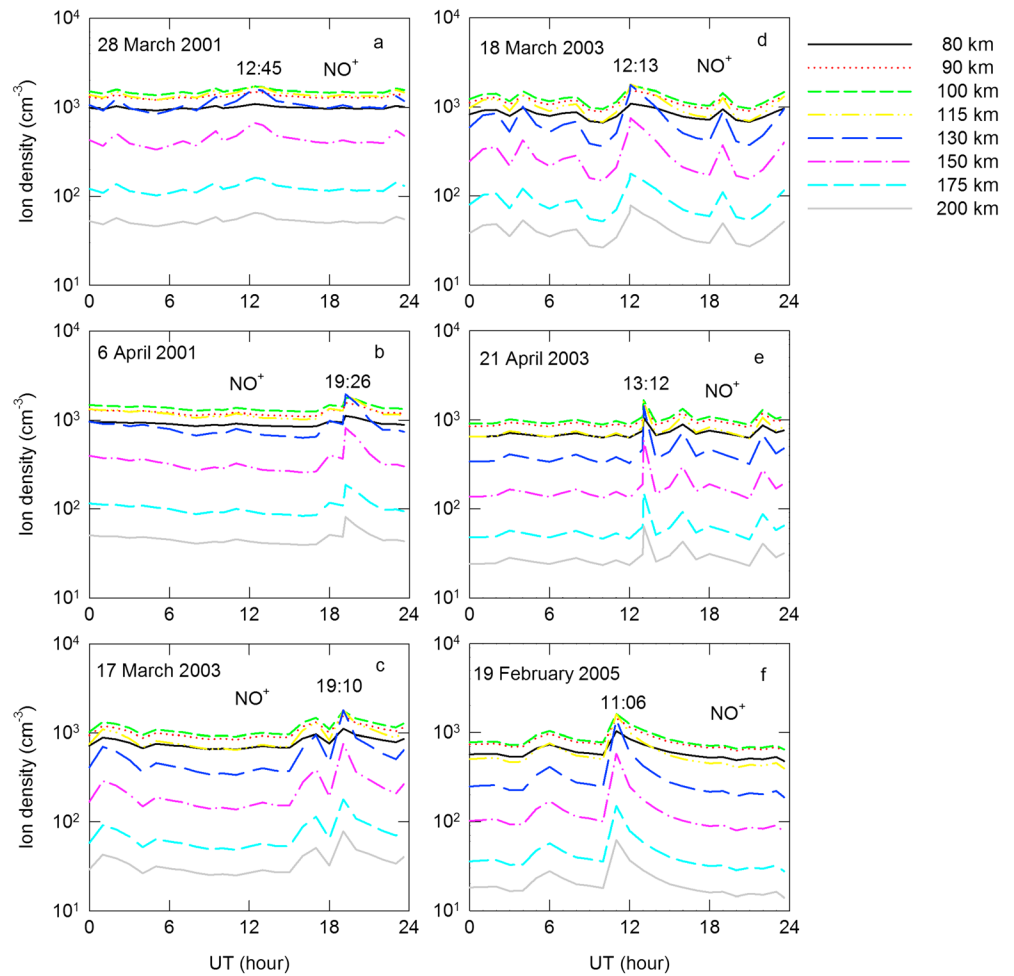


Figure 7. Time series for ion density NO^+ produced by X-ray flares on (a) 28 March 2001, (b) 6 April 2001, (c) 17 March 2003, (d) 18 March 2003, (e) 21 April 2003, and (f) 19 February 2005 in the E region ionosphere of Mars at altitudes 80, 90, 100, 115, 130, 150, 175, and 200 km.

X-rays between wavelength range 10–50 Å [cf. Haider et al., 2002; Mendillo et al., 2006]. We have used solar X-ray flux observed by GOES 10 between wavelength range 1 to 8 Å. Our estimated peak heights of the E region ionosphere are lower by 5–10 km as compared to the measured heights. In Figures 10a, 10e, and 10f the calculated flare peak electron densities for flares of 28 March 2001, 21 April 2003, and 19 February 2005 are lower by a factor of 2 to 5 in comparison to that observed by MGS at the flare time 12:28 UT, 13:17 UT, and 12:24 UT, respectively. In Figures 10b, 10c, and 10d, we have found reasonably good agreement between estimated and measured peak electron densities produced by X-ray flares on 6 April and 17 and 18 March 2001, respectively (compare peak electron densities observed by MGS in Figures 2b–2d at flare time 20:13 UT, 19:38 UT, and 13:17 UT, respectively with the estimated peak electron densities in Figures 10b–10d at the flare time 19:26 UT, 19:10 UT, and 12:13 UT, respectively).

Figures 11a–11f represent a time series of measured and calculated normalized IEC for X-ray flares on 28 March and 6 April 2001, 17 and 18 March and 21 April 2003, and 19 February 2005, respectively (the IEC is normalized with minimum value for each respective day of the flare between 00:00 to 24:00 UT). Before the solar flares occurred, the ionosphere of Mars was calm. Just after the flare an increase of a factor of ~5–10 in the normalized IEC was estimated at 12:45, 19:26, 19:10, 12:13, 13:12, and 11:06 UT on 28 March and 6 April 2001, 17 and 18 March and 21 April 2003, and 19 February 2005, respectively. The decay of the flare continues for a longer time period in comparison to the rise of the flare, so it is possible that the Martian ionosphere can observe this effect after the peak of the flare. Therefore, the effect of X-ray flare

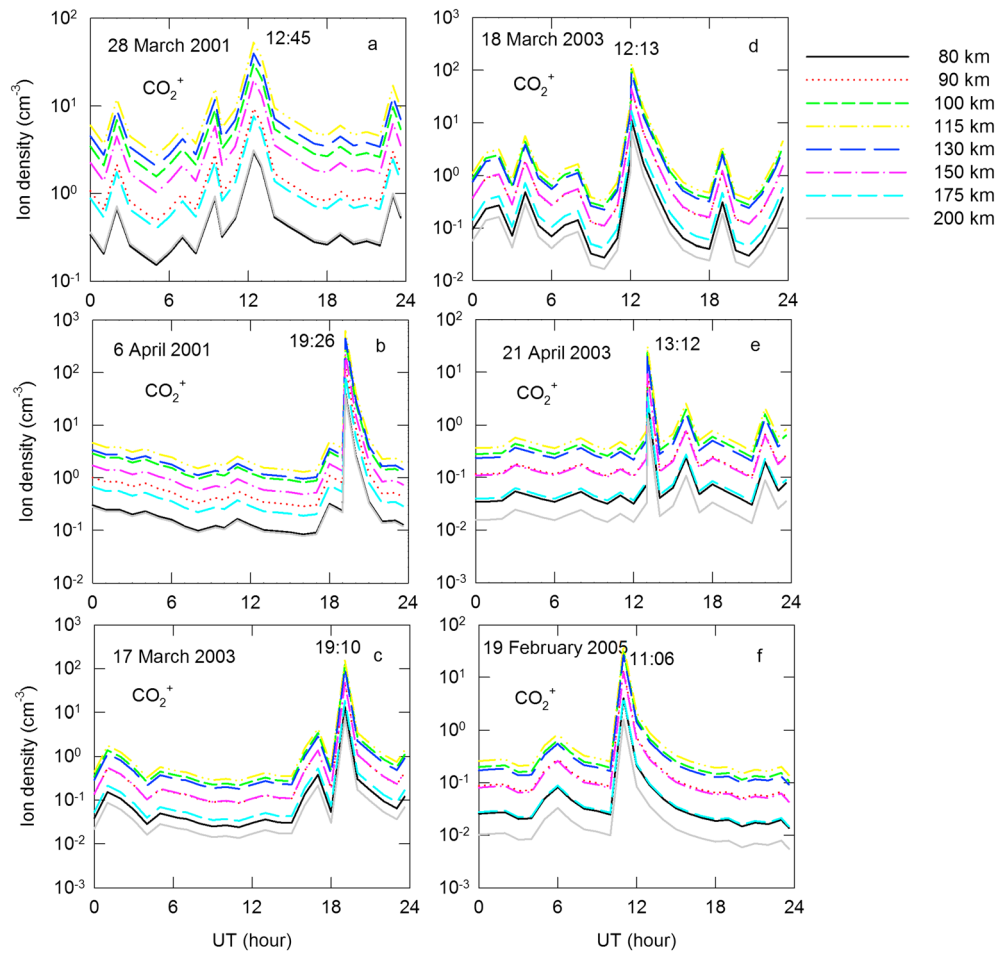


Figure 8. Time series for ion density CO_2^+ produced by X-ray flares on (a) 28 March 2001, (b) 6 April 2001, (c) 17 March 2003, (d) 18 March 2003, (e) 21 April 2003, and (f) 19 February in the E region ionosphere of Mars at altitudes 80, 90, 100, 115, 130, 150, 175, and 200 km.

remains about an hour in the E region ionosphere of Mars. As a result, measured relative IEC increased by a factor of ~ 2.0 at 12:28, 20:13, 19:38, 13:17, 13:17, and 12:24 UT on 28 March and 6 April 2001, 17 and 18 March 2003, and 21 April 2003, and 19 February 2005, respectively. There is a reasonable agreement between measured and estimated IEC during the flare times, considering that the measurement of the IEC was available only during the decay phase of the flares. It should be noted that our estimated IEC values are most consistent with the previous calculated values of Haider et al. [2012] at the flare time. However, a small difference in both calculations at other UTs is not surprising because their atmospheric conditions are not the same. Both calculations are made at different MGS observing conditions.

8. Uncertainty in the Model

The time-dependent AYS model depends on the elastic and inelastic cross sections, photoabsorption and photoionization cross sections, neutral densities, and various chemical reactions. We have taken photoabsorption and photoionization cross sections from different laboratory measurements with uncertainties of 7–12% [cf. Cairns and Samson, 1965; Cook et al., 1966; Lee et al., 1973; McCulloh, 1973; Iida et al., 1986; Watanabe et al., 1967]. The theoretical cross sections for elastic and inelastic collisions are taken from Porter and Jump [1978] and Jackman et al. [1977], respectively. These cross sections were found in good agreement with several investigations and can produce uncertainty about 10% as against the usual experimental uncertainties of 10–15% [cf. Joshipura et al., 2009]. This error can cause 5–7% uncertainties on the model results at energies above 50 eV [Bhardwaj and Jain, 2009]. We have used solar X-ray flux observed

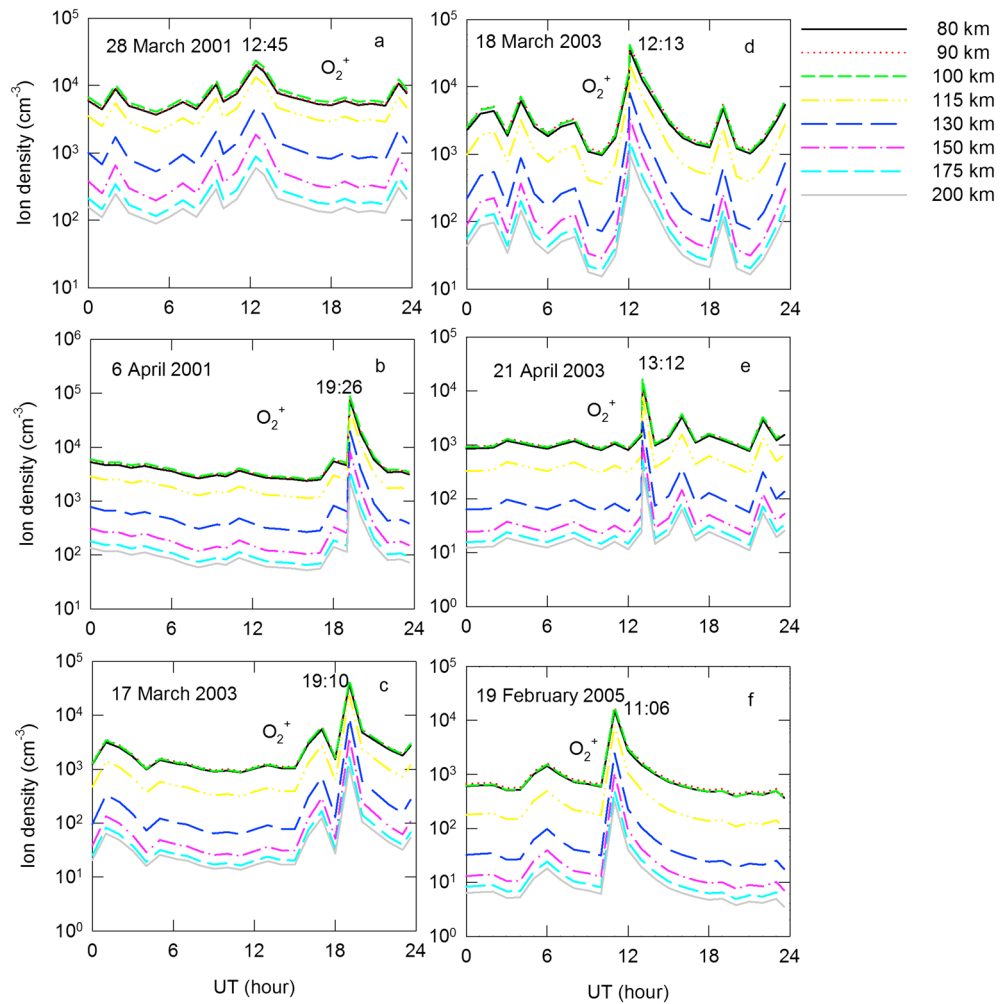


Figure 9. Time series for ion density O_2^+ produced by X-ray flares on (a) 28 March 2001, (b) 6 April 2001, (c) 17 March 2003, (d) 18 March 2003, (e) 21 April 2003, and (f) 19 February 2005 in the E region ionosphere of Mars at altitudes 80, 90, 100, 115, 130, 150, 175, and 200 km.

by GOES at shorter wavelength range 1–8 Å, which has produced ionization peak at about 100 km. This is below the E region peak by 5–10 km. The soft X-ray varies between wavelength range of 1–90 Å [Haider et al., 2011; Haider and Mahajan, 2014]. Using solar fluxes at this wavelength range Haider et al. [2002] estimated mean ionization peak at about 112 km in the E region ionosphere of Mars. There is no measurement of X-ray flux at longer wavelengths during the flare period. Until more observations of X-ray flux at longer wavelengths are not available GOES 1–8 Å flux at shorter wavelength will remain useful for studying the X-ray aeronomy of Mars due to effect of flares in the E region ionosphere. The neutral atmosphere and plasma temperature are not observed for specific days and locations of MGS observations. Therefore, we have used estimated neutral density and plasma temperature with uncertainties of ~5–7% [Millour et al., 2014; Fox, 1993, 2009]. The future measurements of neutral density and plasma temperature will provide better data than what is known at present. The chemistry in the upper atmosphere depends on neutral density and plasma temperature. Therefore, it is expected that ion and electron densities can possibly change when new measurements of neutral density and plasma temperature become available.

Our model does not calculate solar X-ray flux. Therefore, we have used X-ray flux observed by GOES at shorter wavelength range of 1–8 Å. GOES does not observe a full X-ray spectrum at wavelength range of 1–50 Å required for the formation of E layer of the ionosphere. There are existing self-consistent models of ionosphere that can be refined in future to perform such simulations for flare period [Bougher et al., 2004; Gonzalez-Galindo

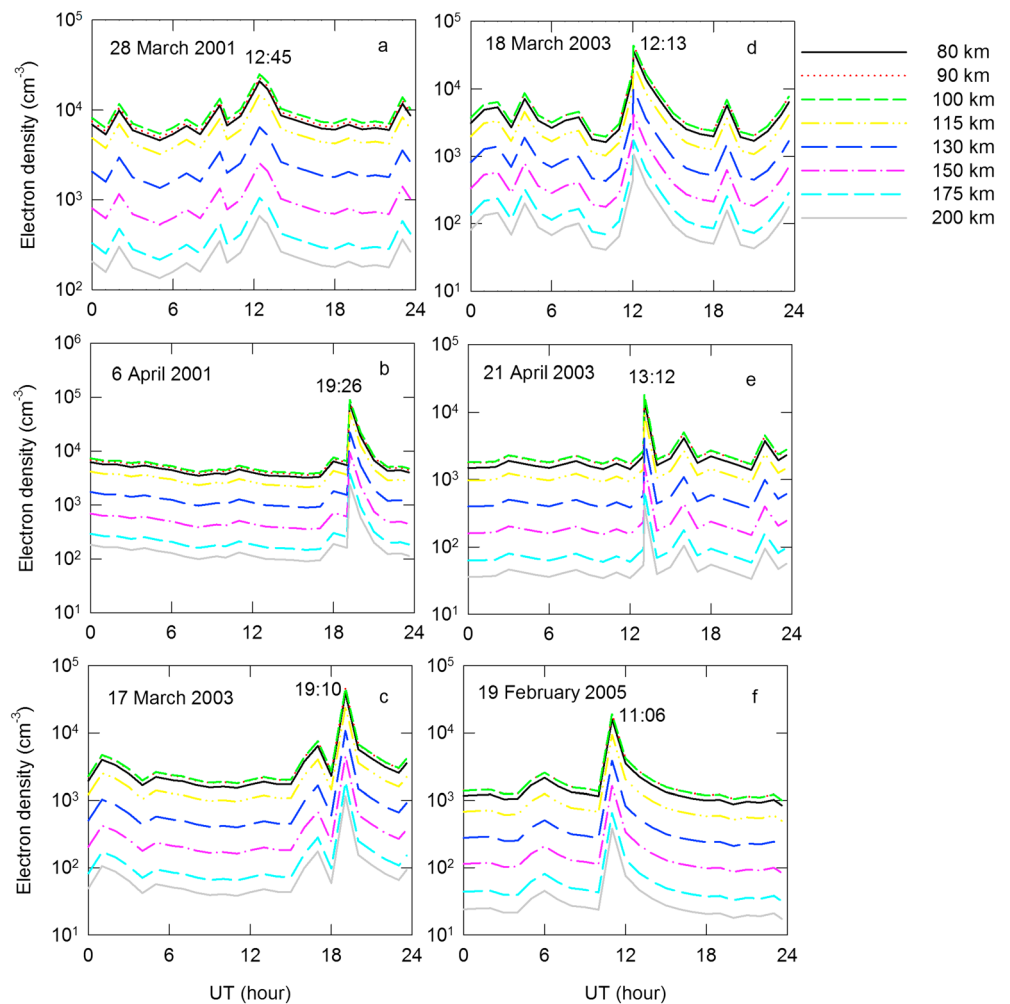


Figure 10. Time series for electron density produced by X-ray flares on (a) 28 March 2001, (b) 6 April 2001, (c) 17 March 2003, (d) 18 March 2003, (e) 21 April 2003, and (f) 19 February 2005 in the *E* region ionosphere of Mars at altitudes 80, 90, 100, 115, 130, 150, 175, and 200 km.

et al., 2011, Haider *et al.*, 2012]. The time-dependent production rates, ion density, electron density, and IEC were not calculated earlier. For the first time, we have developed this model. The transport effect is neglected in our chemical model because this effect is important above 200 km. Our model is useful for studying the time dependent aeronomical processes due to effect of X-ray flares in the *E* region ionosphere of Mars.

9. Conclusion

We have identified six new solar flares that occurred on 28 March and 6 April 2001, 17 and 18 March and 21 April 2003, and 19 February 2005, which have produced enhancement in the electron density of Martian ionosphere. The time series of photoionization rate, photoelectron impact ionization rate, photoelectron flux, ion density, electron density, and IEC have been calculated in the *E* region ionosphere of Mars using GOES X-ray spectra (1–8 Å). We carried out these calculations at fixed SZA for each flare day because electron densities were observed by the MGS at fixed SZA between 00:00–24:00 UT. The production rates, photoelectron flux, and densities increased by 1–2 orders of magnitude due to the effect of these flares in the *E* region ionosphere. The normalized estimated IEC is in reasonable agreement with the normalized IEC observed by the MGS at most of the UT, except at the flare time. It should be noted that the aeronomy of Mars in the *E* region is different from the *F* region ionosphere. The solar flares increased about 200% and 30% ionizations in the *E* and *F* regions as reported by MGS and MEX respectively [cf. Mendillo *et al.*, 2006;

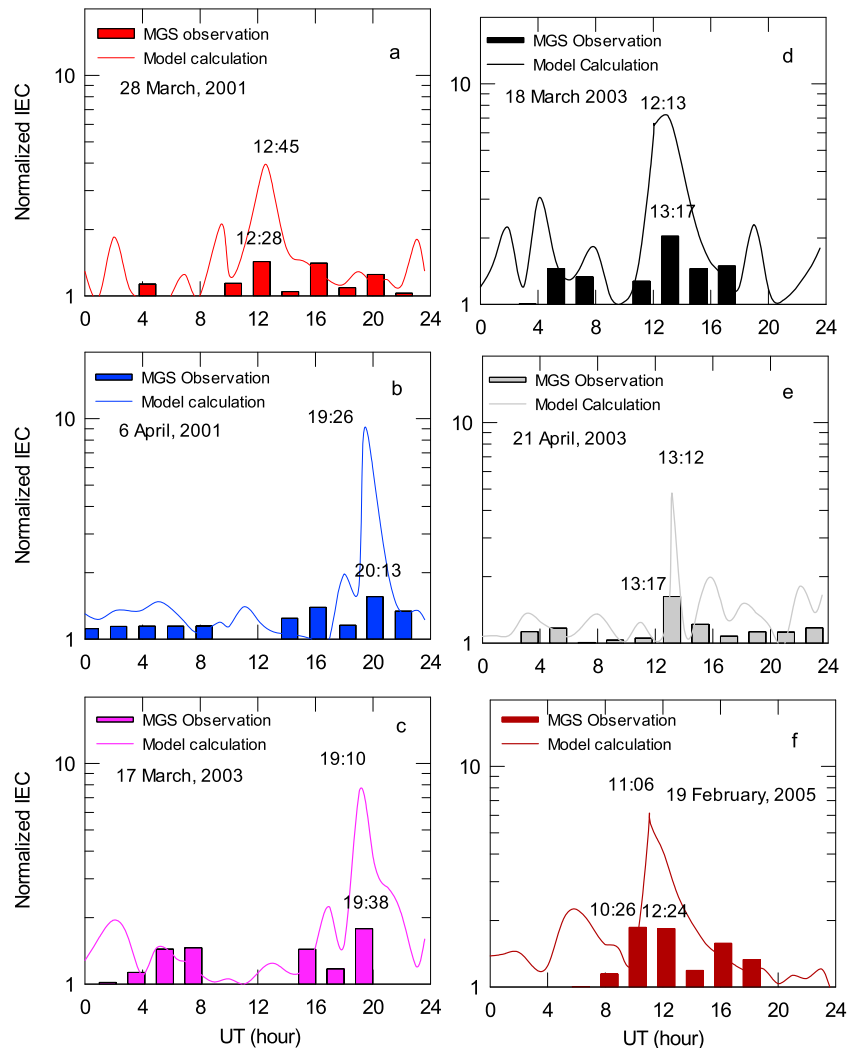


Figure 11. Time series of the normalized IEC estimated and observed by MGS (a) 28 March 2001, (b) 6 April 2001, (c) 17 March 2003, (d) 18 March 2003, (e) 21 April 2003, and (f) 19 February 2005 due to X-ray flares. The peak flare times estimated and observed by MGS are indicated on each curves.

[Nielsen et al., 2006; Haider and Mahajan, 2014]. During solar quiet condition, the E and F peaks were formed in the Martian ionosphere at altitudes ~112–115 km and ~125–145 km due to the impact of X-rays (10–90 Å) and solar EUV (90–1026 Å) radiations, respectively [Haider et al., 2009, 2011]. The E region ionosphere is strongly perturbed due to X-ray flares. The GOES 1–8 Å flux contributed more to the X-ray aeronomy of Mars during flare period. The E-peak production rates and photoelectron fluxes increased by 1–2 orders of magnitudes at flare time. A large increase (by a factor of ~10) in the E-peak density and normalized IEC were obtained due to X-class solar flares that occurred on 6 April 2001 and 17 and 18 March 2003. These enhancements were reduced by ~50% due to M-class solar flares, which occurred on 28 March 2001, 21 April 2003, and 19 February 2005. The normalized IEC obtained from the MGS observations increased by a factor of 2 within 2 h after the flare peak. Thus, a large difference between model and observations can occur, depending upon the time displacement of the measurement with respect to the flare peak time. A large enhancement in the modeled IEC can also be produced due to the use of GOES X-ray flux of wavelength range of 1–8 Å, which contains only a small portion of the X-ray spectrum for generation of the E layer of the ionosphere. The real cause of this difference between observation and model at the flare peak is not fully known. To understand this difference clearly we need measurements of solar X-ray flux at required wavelength range (1–50 Å) and MGS profile of electron density at the flare peak time.

Acknowledgments

MGS data are obtained from archive MGS-M-RSS-5-EDS-V1.0. GOES data are taken from <http://ngdc.noaa.gov/stp/satellite/goes/dataaccess.html>. MCD data are accessible at <http://www-mars.lmd.jussieu.fr>. S.A. Haider thanks the São Paulo Research Foundation (FAPESP): 2014/21995-3. A.M. Santos also thanks FAPESP 2015/25357-4 and PNP/CAPE Space Geophysics Program at INPE.

References

- Anicich, V. G., and W. T. Huntress (1986), A survey of bimolecular ion-molecule reactions for use in modelling the chemistry of planetary atmospheres, cometary comae, and interstellar clouds, *Astrophys. J. Suppl. Ser.*, *62*, 553–672, doi:10.1086/191151.
- Bauer, S. J. (1973), *Physics of Planetary Ionospheres*, Springer, New York.
- Bhardwaj, A., and S. K. Jain (2009), Monte Carlo model of electron energy degradation in a CO₂ atmosphere, *J. Geophys. Res.*, *114*, A11309, doi:10.1029/2009JA014298.
- Biondi, M. A. (1972), Charged particle combination processing, in *Reaction Rate Handbook, DNAI948H*, pp. 16-1, Defence Nucl. Agency, Santa Barbara, Calif.
- Bornmann, P. L., D. Speich, J. Hirman, V. J. Pizzo, R. Grubb, C. Balch, and G. Heckman (1996), The GOES solar X-ray imager: Overview and operational goals, *Proc. SPIE*, *2812*, 309–319, doi:10.1117/12.254078.
- Bougher, S. W., S. Engel, D. P. Hinson, and J. M. Forbes (2001), Mars Global Surveyor radio science electron density profiles: Neutral atmosphere implications, *Geophys. Res. Lett.*, *28*, 3091–3094, doi:10.1029/2001GL012884.
- Bougher, S. W., S. Engel, D. P. Hinson, and J. R. Murphy (2004), Radio science electron density profiles: Interannual variability and implications for the Martian neutral atmosphere, *J. Geophys. Res.*, *109*, E03010, doi:10.1029/2003JE002154.
- Cairns, R. B., and J. A. R. Samson (1965), Absorption and photoionization cross sections of CO₂, CO, Ar, and He at intense solar emission lines, *J. Geophys. Res.*, *70*, 99–104, doi:10.1029/JZ070i001p00099.
- Cook, G. R., P. H. Metzger, and M. Ogawa (1966), Absorption, photoionization and fluorescence of CO, *J. Chem. Phys.*, *44*, 2935–2942, doi:10.1063/1.1727158.
- Dalgarno, A., B. M. McElroy, and R. J. Moffett (1963), Electron temperature in the ionosphere, *Planet. Space Sci.*, *11*, 463–470, doi:10.1016/0032-0633(63)90071-0.
- Fallows, K., P. Withers, and G. Gonzalez (2015), Response of the Mars ionosphere to solar flares: Analysis of MGS radio occultation data, *J. Geophys. Res. Space Physics*, *120*, 9805–9825, doi:10.1002/2015JA021108.
- Fehsenfeld, F. C., and E. E. Ferguson (1972), Thermal energy reaction rate constants for H⁺ and CO⁺, *J. Chem. Phys.*, *56*, 3066–3070, doi:10.1063/1.1677642.
- Fehsenfeld, F. C., A. L. Schmeltekopf, D. B. Dunkin, and E. E. Ferguson (1969), Compilation of reaction rate constants measured in the ESSA flowing afterglow system to August, 1969, *ESSA Tech. Rep. ERL135-AL3*, U.S. Dep. of Comm., Washington, D. C.
- Fehsenfeld, F. C., D. B. Dunkin, and E. E. Ferguson (1970), Rate constants for the reaction of CO₂⁺ with O, O₂ and NO; N₂⁺ with O and NO; and O₂⁺ with NO, *Planet. Space Sci.*, *18*, 1267–1269, doi:10.1016/0032-0633(70)90216-3.
- Ferguson, E. E. (1967), Ionospheric ion-molecule reaction rates, *Rev. Geophys.*, *5*, 305–327, doi:10.1029/RG005i003p00305.
- Ferguson, E. E., F. C. Fehsenfeld, and A. L. Schmeltekopf (1969), Flowing afterglow measurements of ion-neutral reactions, *Adv. At. Mol. Phys.*, *5*, 1–56.
- Fox, J. L. (1993), The production and escape of nitrogen atoms on Mars, *J. Geophys. Res.*, *98*, 3297–3310, doi:10.1029/92JE02289.
- Fox, J. L. (2004), Response of the Martian thermosphere/ionosphere to enhanced fluxes of solar soft X-rays, *J. Geophys. Res.*, *109*, A11310, doi:10.1029/2004JA010380.
- Fox, J. L. (2009), Morphology of the dayside ionosphere of Mars: Implications for ion outflows, *J. Geophys. Res.*, *114*, E12005, doi:10.1029/2009JE003432.
- Fox, J. L., and K. E. Yeager (2006), Morphology of the near-terminator Martian ionosphere: A comparison of models and data, *J. Geophys. Res.*, *111*, A10309, doi:10.1029/2006JA011697.
- Frommhold, L., and M. A. Biondi (1967), Electron temperature dependence of dissociative recombination of Ne⁺ and N₂⁺ ions, *Bull. Am. Phys. Soc.*, *12*, 217–221.
- Golden, D. E., G. Sinnott, and R. N. Varney (1968), Charge transfer cross sections for the reaction N₂⁺ + O₂ → O₂⁺ + N₂ at very low energies, *Phys. Rev. Lett.*, *20*, 239, doi:10.1103/PhysRevLett.20.239.
- Gonzalez-Galindo, F., M. A. Lopez-Valverde, G. Gilli, and F. Forget (2011), Study of the Martian ionosphere with a general circulation model, paper presented at the Fourth International Workshop on Mars Atmosphere: Modeling and Observations, Cent. Natl. DEEtudes Spatiales, Paris, 8–11 Feb.
- Green, A. E. S., C. H. Jackman, and R. H. Garvey (1977), Electron impact on atmospheric gases 2. Yield spectra, *J. Geophys. Res.*, *82*, 5104–5111, doi:10.1029/JA082i032p05104.
- Haider, S. A., and K. K. Mahajan (2014), Lower and upper ionosphere of Mars, *Space Sci. Rev.*, *182*, 19–84, doi:10.1007/s11214-014-0058-2.
- Haider, S. A., and R. P. Singhal (1983), Analytical yield spectrum approach to electron energy degradation in Earth's atmosphere, *J. Geophys. Res.*, *88*, 7185–7189, doi:10.1029/JA088iA09p07185.
- Haider, S. A., J. Kim, A. F. Nagy, C. N. Keller, M. I. Verigin, K. I. Gringauz, N. M. Shutte, K. Szego, and P. Kiraly (1992), Calculated ionization rates, ion densities and airglow emission rates due to precipitating electrons in the nightside ionosphere of Mars, *J. Geophys. Res.*, *97*, 10,637–10,641.
- Haider, S. A., S. P. Seth, E. Kallio, and K. I. Oyama (2002), Solar EUV and electron-proton-hydrogen atom produced ionosphere at Mars: Comparative studies of particle fluxes and ion production rates due to different processes, *Icarus*, *159*, 18–30, doi:10.1006/icar.2002.6919.
- Haider, S. A., M. A. Abdu, I. S. Batista, J. H. Sobral, E. Kallio, W. C. Maguire, and M. I. Verigin (2009), On the responses to solar X-ray flare and coronal mass ejection in the ionospheres of Mars and Earth, *Geophys. Res. Lett.*, *36*, L13104, doi:10.1029/2009GL038694.
- Haider, S. A., V. Sheel, M. Smith, W. Maguire, and G. Molina-Cuberos (2010), Effect of dust storms on the D region of the Martian ionosphere: Atmospheric electricity, *J. Geophys. Res.*, *115*, A12336, doi:10.1029/2010JA016125.
- Haider, S. A., K. K. Mahajan, and E. Kallio (2011), Mars ionosphere: A review of experimental results and modelling studies, *Rev. Geophys.*, *49*, RG4001, doi:10.1029/2011RG000357.
- Haider, S. A., S. M. P. McKenna-Lawlor, C. D. Fry, R. Jain, and K. N. Joshipura (2012), Effects of solar X-ray flares in the E region ionosphere of Mars: First model results, *J. Geophys. Res.*, *117*, A05326, doi:10.1029/2011JA017436.
- Hinson, D. P., R. A. Simpson, J. D. Twicken, G. L. Tyler, and F. M. Flasar (1999), Initial result from radio occultation measurements with Mars Global Surveyor, *J. Geophys. Res.*, *104*, 26,997–27,012, doi:10.1029/1999JE001069.
- Iida, Y., F. Carnovale, S. Daviel, and C. E. Brion (1986), Absolute oscillator-strengths for photoabsorption and the molecular and dissociative photoionization of nitric oxide, *Chem. Phys.*, *105*, 211–225, doi:10.1016/0301-0104(86)80070-2.
- Ikezo, Y., S. Matsuoka, M. Takebe, and A. Viggiano (1986), *Gas Phase Ion-Molecule Reaction Rate Constants Through 1986*, Maruzen Co, Ion Res. Group of the Mass Spectrom. Soc. of Jpn., Tokyo.
- Jackman, C. H., R. H. Garvey, and A. E. S. Green (1977), Electron impact on atmospheric gases I, updated cross sections, *J. Geophys. Res.*, *82*, 5081–5090, doi:10.1029/JA082i032p05081.

- Joshiyura, K. N., S. S. Gangopadhyay, and B. G. Vaishnav (2007), Electron scattering and ionization of NO, N₂O, NO₂, NO₃ and N₂O₅ molecules: Theoretical cross sections, *J. Phys. B*, *40*, 199–210, doi:10.1088/0953-4075/40/1/018.
- Joshiyura, K. N., S. S. Gangopadhyay, H. N. Kothari, and F. A. Shelat (2009), Total electron scattering and ionization of N, N₂ and metastable excited N₂⁺(A₃Σ_u⁺), *Phys. Lett. A*, *373*, 2876–2881, doi:10.1016/j.physleta.2009.05.075.
- Kallio, E., and S. Barabash (2001), Atmospheric effects of precipitating energetic hydrogen atoms on the Martian atmosphere, *J. Geophys. Res.*, *106*, 165–177, doi:10.1029/2000JA002003.
- Kallio, E., K. Liu, R. Jarvinen, V. Pohjola, and P. Janhunen (2010), Oxygen ion escape at Mars in a hybrid model: High energy and low energy ions, *Icarus*, *206*, 152–163, doi:10.1016/j.icarus.2009.05.015.
- Lee, L. C., R. W. Carlson, D. L. Judge, and M. Ogawa (1973), The absorption cross sections of N₂, O₂, CO, NO, CO₂, N₂O, CH₄, C₂H₄, C₂H₆, and C₄H₁₀ from 180 to 700 Å, *J. Quant. Spectrosc. Radiat. Transfer*, *13*, 1023–1031, doi:10.1016/0022-4073(73)90075-7.
- Lollo, A., P. Withers, K. Fallows, Z. Girazian, M. Matta, and P. C. Chamberlin (2012), Numerical simulations of the ionosphere of Mars during a solar flare, *J. Geophys. Res.*, *117*, A05314, doi:10.1029/2011JA017399.
- Ma, Y.-J., et al. (2008), Plasma flow and related phenomena in planetary aeronomy, *Space Sci. Rev.*, *139*, 311–353, doi:10.1007/s11214-008-9389-1.
- Mahajan, K. K., N. K. Lodhi, and S. Singh (2009), Ionospheric effects of solar flares at Mars, *Geophys. Res. Lett.*, *36*, L15207, doi:10.1029/2009GL039454.
- Mantas, G. P., and W. B. Hanson (1987), Analysis of Martian ionosphere and solar wind electron gas data from the planar retarding potential analyzer on the Viking spacecraft, *J. Geophys. Res.*, *92*, 8559–8569, doi:10.1029/JA092iA08p08559.
- Martinis, C. R., J. K. Wilson, and M. J. Mendillo (2003), Modeling day-to-day ionospheric variability on Mars, *J. Geophys. Res.*, *108*(A10), 1383, doi:10.1029/2003JA009973.
- McCulloh, K. E. (1973), Photoionization of carbon dioxide, *J. Chem. Phys.*, *59*, 4250, doi:10.1063/1.1680619.
- McFarland, M., D. L. Albritton, F. C. Fehsenfeld, A. L. Schmeltekopf, and E. E. Ferguson (1974), Energy dependence of rate constant for the reaction O⁺ + NO → NO⁺ + O, *J. Geophys. Res.*, *79*, 2005, doi:10.1029/JA079i013p02005.
- Mendillo, M., P. Withers, D. Hinson, H. Rishbeth, and B. Reinisch (2006), Effects of solar flares on the ionospheres of Mars, *Science*, *311*, 1135–1138, doi:10.1126/science.1122099.
- Millour, E., et al. (2014), A new Mars climate database v5.1, paper 1301 presented at The Fifth International Workshop on Mars Atmosphere: Modeling and Observations, Oxford, U. K., Jan. 2014.
- Mitchell, D. L., R. P. Lin, H. Reme, D. H. Crider, P. A. Cloutier, J. E. P. Connerney, M. H. Acuna, and N. F. Ness (2000), Oxygen auger electrons observed in Mars' ionosphere, *Geophys. Res. Lett.*, *27*, 1871–1874, doi:10.1029/1999GL010754.
- Molina-Cuberos, G. J., H. Lichtenegger, K. Schwingenschuh, J. J. Lopez-Moreno, and R. Rodrigo (2002), Ion-neutral chemistry model of the lower ionosphere of Mars, *J. Geophys. Res.*, *107*(E5), 5027, doi:10.1029/2000JE001447.
- Mul, P. M., and J. W. McGowan (1979), Temperature dependence of dissociative recombination for atmospheric ions NO, O₂, and N₂, *J. Phys. B*, *12*, 1591–1601, doi:10.1088/0022-3700/12/9/011.
- Nagy, A. F., and P. M. Banks (1970), Photoelectron fluxes in the ionosphere, *J. Geophys. Res.*, *75*, 6260–6270, doi:10.1029/JA075i031p06260.
- Nagy, A. F., et al. (2004), The plasma environment of Mars, *Space Sci. Rev.*, *111*, 33–114, doi:10.1023/B:SPAC.0000032718.47512.92.
- Ness, N. F., M. H. Acuña, J. E. P. Connerney, A. J. Kliore, T. K. Breus, A. M. Krymskii, P. Cloutier, and S. J. Bauer (2000), Effects of magnetic anomalies discovered at Mars on the structure of the Martian ionosphere and solar wind interaction as follows from radio occultation experiments, *J. Geophys. Res.*, *105*, 15,991–16,004, doi:10.1029/1999JA000212.
- Nielsen, E., H. Zou, D. A. Gurnett, D. L. Kirchner, D. D. Morgan, R. Huff, R. Orosei, A. Safaieinili, J. J. Plaut, and G. Picardi (2006), Observations of vertical reflections from the topside Martian ionosphere, *Space Sci. Rev.*, *126*, 373–388, doi:10.1007/s11214-006-9113-y.
- Nogueira, P. A. B., et al. (2015), Modeling the equatorial and low-latitude ionospheric response to an intense X-class solar flare, *J. Geophys. Res. Space Physics*, *120*, 3021–3032, doi:10.1002/2014JA020823.
- Pandya, B. M., and S. A. Haider (2014), Numerical simulation of the effects of Meteoroid ablation and solar EUV/X-ray radiation in the dayside ionosphere of Mars: MGS/MEX observations, *J. Geophys. Res. Space Physics*, *119*, 9228–9245, doi:10.1002/2014JA020063.
- Porter, H. S., and F. W. Jump (1978), Analytical total and angular elastic electron impact cross sections for planetary atmospheres, *Tech. Rep. CSC/TM-78/0017*, Comput. Sci. Corp., Greenbelt, Md.
- Qian, L., A. G. Burns, S. C. Solomon, and P. C. Chamberlin (2012), Solar flare impacts on ionospheric electrodynamics, *Geophys. Res. Lett.*, *39*, L06101, doi:10.1029/2012GL051102.
- Rastogi, R. G., B. M. Pathan, D. R. K. Rao, T. S. Sastry, and J. H. Sastri (1999), Solar flare effects on the geomagnetic elements during normal and counter electrojet periods, *Earth Planets Space*, *51*, 947–957, doi:10.1186/BF03351565.
- Seth, S. P., S. A. Haider, and K. I. Oyama (2002), The photoelectron flux and nightglow emissions of 5577 Å and 6300 Å due to solar wind electron precipitation in Martian atmosphere, *J. Geophys. Res.*, *107*(A10), 1324, doi:10.1029/2001JA000261.
- Seth, S. P., V. B. Rao, C. M. Espirito Santo, S. A. Haider, and V. R. Choksi (2006), Zonal variation of peak ionization rates in upper atmosphere of Mars at high latitude using Mars Global Surveyor Accelerometer data, *J. Geophys. Res.*, *111*, A09308, doi:10.1029/2006JA011753.
- Singhal, R. P., and A. E. S. Green (1981), Spatial aspects of electron energy degradation in atmospheric oxygen, *J. Geophys. Res.*, *85*, 4776–4780, doi:10.1029/JA086iA06p04776.
- Singhal, R. P., and S. A. Haider (1984), Analytical yield spectrum approach to photoelectron fluxes in the Earth's atmosphere, *J. Geophys. Res.*, *89*, 6847–6852, doi:10.1029/JA089iA08p06847.
- Singhal, R. P., C. H. Jackman, and A. E. S. Green (1980), Spatial aspects of low and medium energy electron degradation in N₂, *J. Geophys. Res.*, *85*, 1246–1254, doi:10.1029/JA085iA03p01246.
- Smith, F. L., and C. Smith (1972), Numerical evaluation of Chapman's grazing incidence integral Ch (X, chi), *J. Geophys. Res.*, *77*, 3592–3597, doi:10.1029/JA077i019p03592.
- Sripathi, S., N. Balachandran, B. Veenadhari, R. Singh, and K. Emperumal (2013), Response of the equatorial and low-latitude ionosphere to an intense X-class solar flare (X7/2B) as observed on 09 August 2011, *J. Geophys. Res. Space Physics*, *118*, 2648–2659, doi:10.1002/jgra.50267.
- Thomson, N. R., C. J. Rodger, and R. L. Dowden (2004), Ionosphere gives size of greatest solar flare, *Geophys. Res. Lett.*, *31*, L06803, doi:10.1029/2003GL019345.
- Torr, D. G., and M. R. Torr (1979), Chemistry of the thermosphere and ionosphere, *J. Atmos. Terr. Phys.*, *41*, 797–839, doi:10.1016/0021-9169(79)90126-0.
- Walls, F. L., and G. H. Dunn (1974), Measurement of total cross sections for electron recombination with NO⁺ and O₂⁺ using ion storage techniques, *J. Geophys. Res.*, *79*, 1911–1915, doi:10.1029/JA079i013p01911.
- Watanabe, K., F. M. Matsunaga, and H. Sakai (1967), Absorption coefficient and photoionization yield of NO in the region 580–1350 Å, *Appl. Opt.*, *6*, 1220, doi:10.1364/AO.6.001220.
- Withers, P., M. Mendillo, D. P. Hinson, and K. Cahoy (2008), Physical characteristics and occurrence rates of meteoric plasma layers detected in the Martian ionosphere by the Mars Global Surveyor Radio Science Experiment, *J. Geophys. Res.*, *113*, A12314, doi:10.1029/2008JA013636.
- Xiong, B., et al. (2011), Ionospheric response to the X-class solar flare on 7 September 2005, *J. Geophys. Res.*, *116*, A11317, doi:10.1029/2011JA016961.